Article

A charge-maintaining ATRP initiator rescues the lost function of negatively charged protein-polymer conjugates

Stefanie L Baker, Hironobu Murata, Bibifatima Kaupbayeva, Adina Tasbolat, Krzysztof Matyjaszewski, and Alan J Russell

Biomacromolecules, **Just Accepted Manuscript** • DOI: 10.1021/acs.biomac.9b00379 • Publication Date (Web): 13 May 2019

A charge-maintaining ATRP initiator rescues the lost function of negatively charged protein-polymer conjugates

Stefanie L. Baker,[1,2**] Hironobu Murata,[2**] Bibifatima Kaupbayeva[2,3], Adina Tasbolat[4], Krzysztof Matyjaszewski[2,5], Alan J. Russell[*1,2,5,6,7]

[1]Department of Biomedical Engineering, Scott Hall 4N201, Carnegie Mellon University, 5000 Forbes Avenue, Pittsburgh, PA 15213, United States

[2]Center for Polymer-Based Protein Engineering, Carnegie Mellon University, 5000 Forbes Avenue, Pittsburgh, PA 15213, United States

[3]Department of Biological Sciences, Carnegie Mellon University, 4400 Fifth Avenue, Pittsburgh, PA 15213, United States

[4]Department of Chemistry and Chemical Technology, Al-Farabi Kazakh National University, 71 Al-Farabi Avenue, Almaty, 050040, Republic of Kazakhstan

[5]Department of Chemistry, Carnegie Mellon University, 4400 Fifth Avenue, Pittsburgh, PA 15213, United States

[6]Disruptive Health Technology Institute, Carnegie Mellon University, 5000 Forbes Avenue, Pittsburgh, PA 15213, United States

[7]Department of Chemical Engineering, Carnegie Mellon University, 5000 Forbes Avenue, Pittsburgh, PA 15213, United States

**These authors contributed equally to this work

ABSRACT

When grown from the surface of proteins, negatively charged polymers cause irreversible inactivation, thereby limiting the breadth of the synthetic space that negatively charged protein-polymer conjugates can be applied to. More broadly speaking, independent of polymer and synthetic approach, almost all protein-polymer conjugates are less active than their precursors. After more than a decade without major advances in understanding why the attachment of some polymers so sharply deactivates enzymes, we focused our attention on a technique to protect enzymes from the growth of a deactivating polymer by restoring the charge at the protein surface during polymer attachment. We synthesized an amino-reactive positively-charged ATRP initiator that inserted a permanent positive charge at the site of bio-macroinitiator attachment. Maintaining surface charge through attachment of the permanent positively charged initiator led to the first observation of activity of enzymes that were coupled to negatively charged homopolymers.

Keywords: charged initiator, ATRP, protein-polymer conjugate, surface charge

The delicate balance of forces that maintain the structure, function, and dynamics of enzymes is at the heart of their remarkable activity and bothersome instability.[1] Although some enzymes have evolved to survive in extreme environments[2], protein engineers that desire to stabilize proteins for therapeutic or industrial uses have generally used molecular biology to dramatically improve function.[3–5] Another compelling approach to protein/enzyme stabilization has been to covalently attach polymers to the protein surface.[6–9] Polymers can either be covalently coupled to the surface of proteins (commonly referred to as PEGylation; PEG=poly(ethylene glycol)) or grown from the surface of proteins using controlled radical polymerization from protein-initiator constructs, also known as bio-macroinitiators.[10–20] ATRP has been used to grow dense polymer coatings that "nano-armor" proteins.[21,22] A wide variety of polymers, over a range of molecular weights and densities, have been conjugated with proteins to determine their impact on function, including random copolymers[23], block copolymers[24–26], thermoresponsive[10,13,27] or pH responsive polymers[28], branched polymers[29], and charged polymers.[9,30,31] Unfortunately, however, the full diversity of polymers that can be attached to proteins is inaccessible because some polymers almost instantaneously unfold and inactivate proteins. In particular, the growth of negatively charged polymers from the surface of enzymes is not tolerated by proteins.[32]

Interestingly, even while the conjugation of conventional PEG to a protein increases its stability, it is always at the expense of bioactivity.[33] Protecting proteins from conjugated polymer-induced activity loss is a vexing challenge in the field of next generation protein-polymer conjugate design.[34] Since Jiang's work in 2011, zwitterionic polymers have become increasingly attractive for protein conjugation because they improve stability while preserving some degree of bioactivity.[35] Zwitterionic monomers have a one-to-one ratio of positively and

negatively charged groups yielding a net neutral molecule and their polymeric forms were found to be stabilizing for proteins by mimicking stabilizing kosmotropic anions and chaotropic cations as defined by the Hofmeister series.[35,36] Previous studies by our group have shown the stabilizing effect of zwitterionic poly(carboxybetaine methacrylate) (pCBMA) along with high stabilities and activity retention with positively charged polymers, such as poly(quaternary ammonium methacrylate) (pQA).[9,32] These polymers contain stabilizing chaotropic cations, NH_4^+, aligning with the findings of Jiang. We also found that at low pH, these polymers could act as powerful intramolecular chaperones to drive protein folding and stabilization.[32] We have also shown, however, that negatively charged polymers, such as poly(sulfonate methacrylate) (pSMA), are destabilizing and deactivating.[16,32] pSMA is a hydrophilic, negatively charged polymer containing kosmotropic sulfonate anions, as shown in **Scheme 1**, which are defined as stabilizing by the Hofmeister series. Another study used the SMA monomer, copolymerized with three other monomers of varying hydrophobicities, and found the random heteropolymer to be stabilizing due to statistical monomer distribution.[23] The first publication by our group on grafted-from protein-polymer conjugates used a negatively charged homopolymer, poly(sodium 4-styrenesulfonate) to create conjugates with α-chymotrypsin (CT) that also sharply reduced enzyme activity.[8] To our knowledge, there are no reported protein-negatively charged homopolymer conjugates that maintain enzyme stability or activity. Determining why negatively charged homopolymers are deactivating and destabilizing to proteins may enable us to remediate the problem and then use that knowledge to determine if more general protein conjugate-induced activity loss can be reduced when using compatible polymers.

In order to design a polymer conjugation protective strategy, we have focused our attention on how ATRP initiators are coupled to proteins. Our prior work has always focused on

the properties of next generation protein-polymer conjugates, but in doing that work, we routinely used protein macroinitiator constructs as controls. We have observed that although compatible polymers can stabilize enzymes, their biomacromolecular initiator precursors are often less active and stable than the native protein or the conjugate.[32] Protein-initiator constructs are most often formed by reacting accessible surface amino groups with activated ester alkyl halides. These reactions, and almost all common PEGylation coupling chemistries, sacrifice the native electrostatic environment of the protein surface for the supposed benefit of the resulting protein-polymer conjugate (**Figure S1 and Table S1**). The prevailing view of protein scientists has been that maintaining protein surface charge-charge interactions is less important to protein stability than maintaining the integrity of the hydrophobic core. Indeed, hydrophobic interactions within a protein contribute hundreds of kJ mol^{-1} to maintaining a folded conformation, whereas exposed surface charge-charge interactions only contribute a few kJ mol^{-1}.[37–40] Surprisingly, however, rationally optimizing charge-charge interactions can be an effective tool when designing proteins with increased stability.[41–47] These charge-charge interactions can either be optimized by increasing favorable electrostatic interactions or by decreasing the number of unfavorable electrostatic interactions.[48] It has also been observed that long-range electrostatic interactions are just as important as short-range salt bridge interactions.[47] Conversely, others have questioned whether charge-charge interactions are important influencers of stability.[49] Commercially, of the 14 FDA-approved therapeutic protein-polymer conjugates, Neulasta and Plegridy are the only two examples where the nitrogen is still positively charged after PEG attachment by utilizing aldehyde attachment chemistries that result in secondary amines (**Figure S1 and Table S1**). Two natural questions arise: could we protect an enzyme from the growth of an incompatible polymer by initiating the reaction from a charge-maintaining initiator? And, if

so, could that same strategy be used to further enhance the activity and stability of compatible polymer-protein conjugates?

Modeled after successfully commercialized PEGylation reagents, alkyl halide ATRP-initiators usually possess *N*-hydroxysuccinimide (NHS) groups that react with protein primary amines, including the N-terminal and lysine residues. We have developed algorithms that can predict the site of reaction on the protein surface as well as the initiation reaction rates at each amino group.[50] The amino group on the N-terminus has a pK_a in the range of 7.8-8.0 while the pK_a's of lysine side chain amino groups range from approximately 10.5-12.0, depending on their local environment.[51] Therefore, at biologically relevant pH values (6-8), all accessible amino groups will be positively charged almost all of the time (>95%). These positive charges are unfortunately lost when neutral initiators are used to launch protein-ATRP as the nitrogens are converted to amide bonds.[52,53]

We hypothesized that a positively charged ATRP-initiator would restore the positive charges on an enzyme surface, thereby enhancing activity and stability of the enzyme-initiator constructs and the protein-polymer conjugates derived from it. We describe the synthesis of the first positively charged amine-reactive ATRP-initiator. We used this initiator to study the growth of an incompatible polymer (pSMA) from the surfaces of α-chymotrypsin (CT), uricase, acetylcholinesterase, lysozyme, and avidin. We now understand that the charge of an ATRP-initiator is a crucial parameter to consider in the design of highly active and stable protein-polymer conjugate variants and that negatively charged polymers can now lead to conjugates with high activities and stabilities.

MATERIALS AND METHODS

Materials α-chymotrypsin (CT) from bovine pancreas (type II), acetylcholinesterase (AChE) from *Electrophorus electricus* (electric eel, type VI-S), uricase from Candida sp., lysozyme from chicken egg white, biotin, and HABA 4'-hydroxyazobenzene-2-carboxylic acid were purchased from Sigma Aldrich (St. Louis, MO). Avidin from egg white was purchased from Lee Biosolutions (Maryland Heights, MO). CT, lysozyme, and avidin were used as received. AChE and uricase were dialyzed in 25 mM sodium phosphate (pH 7.0) using a 25 kDa molecular weight cutoff dialysis tube in a refrigerator for 24 h and were then lyophilized. Copper (II) chloride, sodium ascorbate, 1,1,4,7,10,10-hexamethyltriethylenetetramine (HMTETA), 2-bromo-2-methylpropionyl bromide, 3-(dimethylamino)-1-propylamine, *N,N'*-diisopropylcarbodimine, fluorescamine, acetylthiocholine iodide, and 5,5'-dithiobis(2-nitrobenzoic acid) (DTNB) were purchased from Sigma Aldrich. 4-bromobutyric acid and *N*-hydroxysuccinimide were purchased from TCI USA (Portland, OR). Micro BCA assay kit was purchased from Thermo Fisher Scientific.

Instrumentation and Sample Analysis Preparations

^{1}H and ^{13}C NMR were recorded on a spectrometer (500 MHz, 125 MHz, Bruker Avance™ 500) in the NMR facility located in the Center for Molecular Analysis, Carnegie Mellon University, Pittsburgh, PA, with deuterium oxide (D_2O) and DMSO-d_6. Routine FT-IR spectra were obtained with a Nicolet Avatar 560 FT-IR spectrometer (Thermo) in the Department of Chemical Engineering at Carnegie Mellon University. Ultraviolet-visible (UV−VIS) spectra were obtained and used for enzyme activity determination using an UV−VIS spectrometer (Lambda 45, PerkinElmer) with a temperature-controlled cell holder. Melting points (mp) were measured with a Laboratory Devices Mel-Temp. Number and weight average molecular weights (M_n and M_w) and the polydispersity index (M_w/M_n) were estimated by gel permeation chromatography (GPC)

on a Water 2695 Series with a data processor, equipped with three columns (Waters Ultrahydrogel Linier, 500 and 250), using Dulbecco's Phosphate Buffered Saline with 0.02 wt% sodium azide for pCBMA and 80 vol% of 100 mM sodium phosphate (pH 9.0) and 20 vol% of acetonitrile for pSMA as an eluent at flow rate of 1.0 mL/min, with detection by a refractive index (RI) detector. Pullulan standards (PSS-Polymer Standards Service – USA Inc, Amherst, MA) were used for calibration. Matrix-Assisted Laser Desorption Ionization Time-of-Flight Spectrometry (MALDI-ToF MS) was performed with a Perseptive Biosystems Voyager Elite MALDI-ToF spectrometer in the Center for Molecular Analysis, Carnegie Mellon University. Dynamic Light Scattering (DLS) data were collected on a Malvern Zetasizer nano-ZS, which was located in the Department of Chemistry, Carnegie Mellon University. The concentration of the sample solution was kept at 0.2 - 1.0 mg/mL. The hydrodynamic diameters of samples were measured three times (15 runs for each measurement).

Positive initiator synthesis and characterization

4-bromobutyryl-*N*-oxysuccinimide ester synthesis

N,N'-diisopropylcarbodimine (8.5 mL, 55 mmol) was slowly added to the solution of 4-bromobutyric acid (8.4 g, 50 mmol) and *N*-hydroxysuccinimide (4.3 g, 55 mmol) in dichloromethane (100 mL) at 0 °C, and then the mixture was stirred at room temperature overnight. Precipitated urea was filtered out and the filtrate was evaporated to remove the solvent. 4-bromobutyryl-*N*-oxysuccinimine ester was isolated by recrystallization in 2-propanol; yield 10.2 g (77 %), mp 49 – 52 °C. ^{1}H NMR (500 MHz, DMSO-d_6) δ 2.16 (m, 2 H, C=OCH$_2$CH_2CH$_2$Br), 2.81 (s, 4 H, succinimide), 2.83 (t, 2 H, J = 7.0 Hz, C=OCH_2CH$_2$CH$_2$Br), 3.60 (t, 2 H, J = 7.0 Hz, C=OCH$_2$CH$_2$CH_2Br) ppm; ^{13}C NMR (125 MHz, DMSO-d_6) δ 25.9, 27.9,

29.5, 33.3, 168.7, 170.6 ppm; IR (KBr pellete) 3017, 2948, 2914, 2852, 1812, 1786, 1731, 1382, 1360, 1311, 1202 and 1150 cm^{-1}.

_N_-(3-_N'_,_N'_-Dimethylaminopropyl)-2-bromoisobutyramide synthesis

2-bromo-2-methylpropionyl bromide (3.4 mL, 27 mmol) was slowly added into the solution of 3-(dimethylamino)-1-propylamine (3.1 mL, 24.6 mmol) in deionized water (50 mL) at 0 °C, and then the mixture was stirred at room temperature for 1 h. After the mixture was adjusted to pH 10 with 5 N NaOH aq. at 0 °C, the product was extracted with ethyl acetate (50 mL x 3). The organic phase was washed with 20 wt% potassium carbonate aq. (50 mL × 3) and saturated NaCl aq. (50mL × 2). The organic phase was dried with Na_2CO_3 and evaporated to remove the solvent. *N*-(3-*N',N'*-Dimethylaminopropyl)-2-bromoisobutyramide was isolated *in vacuo*. oil compound; yield 5.9 g (95 %), ^{1}H NMR (500 MHz, DMSO-d_6) δ 1.56 (m, 2 H, $(CH_3)_2NCH_2CH_2CH_2NHC{=}O$), 1.84 (s, 6 H, $C{=}OC(CH_3)_2Br$), 2.11 (s, 6 H, $(CH_3)_2NCH_2CH_2$), 2.22 (t, 2 H, J = 7.0 Hz, $(CH_3)_2NCH_2CH_2$), 3.12 (td, 2 H, J = 5.5 Hz and J = 7.0 Hz, $CH_2CH_2NHC{=}O$), 8.20 (broad t, 1 H, J = 5.5 Hz, amide) ppm; ^{13}C NMR (125 MHz, DMSO-d_6) δ 26.7, 31.6, 38.7, 45.5, 57.4, 61.5, 170.9 ppm; IR (NaCl plate) 3349, 2975, 2946, 2864, 2822, 2800, 1661, 1537, 1465, 1370, 1294, 1263, 1195, 1161 and 1113 cm^{-1}.

Positively charged ATRP initiator synthesis

N-(3-*N',N'*-Dimethylaminopropyl)-2-bromoisobutyramide (1.9 g, 7.5 mmol) and 4-bromobutyryl-*N*-oxysuccinimide ester (2.0 g, 7.5 mmol) were added in dried acetonitrile (50 mL) and bubbled with nitrogen gas for 10 min. The mixture was sealed and stirred at 40 °C overnight. The positively charged ATRP initiator (**1**) was precipitated in a mixture of ethyl acetate and diethyl ether (1:1 volume ratio), and the oil compound was isolated *in vacuo*; yield

3.6 g (93 %) (**Figure S2**), ^{1}H NMR (500 MHz, D_2O) δ 1.88 (s, 6 H, C=OC(CH_3)$_2$Br), 1.91 – 2.24 (m, 4 H, C=OCH$_2$CH_2CH$_2$N$^+$CH$_2$CH_2CH$_2$NHC=O), 2.83 – 2.93 (m, 9 H, succinimide and C=OCH_2CH$_2$CH$_2$N$^+$(CH_3)), 3.04 – 3.14 (m, 5 H, C=OCH$_2$CH$_2$CH_2N$^+$(CH_3)), 3.28 – 3.41 (m, 4 H, N$^+$CH_2CH$_2$CH_2NHC=O) ppm (**Figure S3**); ^{13}C NMR (125 MHz, D_2O) δ22.1, 24.0, 25.6, 30.6, 36.6, 42.9, 51.1, 55.4, 61.6, 62.1, 169.1, 173.2, 174.9 ppm (**Figure S4**); IR (NaCl plate) 3418, 2969, 2708, 1813, 1780, 1734, 1653, 1536, 1472, 1371, 1298, 1210, 1113 and 1074 cm^{-1}.

Electrospray ionization mass spectrometry (ESI-MS)

The positive initiator was characterized with ESI-MS using a Finnigan LCQ (Thermo Fisher) quadrupole field ion trap mass spectrometer with an electrospray ionization source (**Figure S5**). Each scan was acquired over 150-2000 m/z using a step of 0.5 u, dwell time of 1.5 ms, mass defect of 50 pu, and 80 V orifice potential. The positive initiator was dissolved in methanol at 100 μM and eluted using methanol at a flow rate of 15 μL/min.

Protein-initiator synthesis and characterization

Chymotrypsin (CT): 200 μL of NHS-functionalized ATRP initiator solution in DMSO (168 μmol, 56 mg for neutral and 87 mg for positive initiator, respectively) was added to a CT solution (60 mg in 30 mL of 100 mM sodium phosphate buffer (pH 8.0)) and stirred at 4 °C for 2 h. CT-initiator conjugates were dialyzed in deionized water using a 15 kDa molecular weight cutoff dialysis tube in a refrigerator for 24 h and were then lyophilized.

Lysozyme: 200 μL of NHS-functionalized ATRP initiator solution in DMSO (172 μmol, 58 mg for neutral and 89 mg for positive initiator, respectively) was added to a lysozyme solution (70 mg in 30 mL of 100 mM sodium phosphate buffer (pH 8.0)) and stirred at room temperature for 2 h. Lysozyme-initiator conjugates were dialyzed in deionized water using an 8 kDa molecular weight cutoff dialysis tube in a refrigerator for 24 h and were then lyophilized.

Avidin: Neutral initiator (21 mg, 0.063 mmol) and avidin (20 mg, 0.0013 mmol protein, 0.013 mmol primary amine groups) were dissolved in 4 mL of 0.1 M sodium phosphate buffer (pH 8). The positively charged ATRP initiator (27 mg, 0.063 mmol) was dissolved in 50 μL of DMSO and added to a solution of avidin (20 mg, 0.013 mmol primary amine groups) in 4 mL of 0.1 M sodium phosphate buffer (pH 8). The solutions were stirred at 4°C for 2 h and avidin conjugates were purified by dialysis using 15 kDa molecular weight cutoff dialysis tube, in 25 mM sodium phosphate (pH 8), for 24 h at 4°C and were then lyophilized.

Uricase: 200 μL of NHS-functionalized ATRP initiator solution in DMSO (100 μmol, 34 mg for neutral and 52 mg for positive initiator, respectively) was added to a uricase solution (20 mg of uricase in 20 mL of 100 mM sodium phosphate buffer (pH 7.0)) and stirred at room temperature for 2 h. Uricase-initiator conjugates were dialyzed in 25 mM sodium phosphate (pH 7.0) using a 25 kDa molecular weight cutoff dialysis tube in a refrigerator for 24 h and were then lyophilized. The concentration of protein in the uricase-initiator conjugate was determined using a Micro BCA Assay Kit (ThermoFisher Scientific).

Acetylcholinesterase (AChE): 100 μL of NHS-functionalized ATRP initiator solution in DMSO (12.7 μmol, 4.3 mg for neutral and 5.5 mg for positive initiator, respectively) was added to an AChE solution (7 mg of AChE in 10 mL of 100 mM sodium phosphate buffer (pH 7.0)) and stirred at room temperature for 2 h. AChE-initiator conjugates were dialyzed in 25 mM sodium phosphate buffer (pH 7.0) using a 25 kDa molecular weight cutoff dialysis tube in a refrigerator for 24 h and were then lyophilized. The concentration of protein in the AChE-initiator conjugate was determined using a Micro BCA Assay Kit.

BCA protein assay

The concentration of protein in the solution was determined using a Micro BCA protein Assay Kit (ThermoFisher Scientific). The sample solution (25 μL) and Micro BCA working reagent

(75 μL) were incubated at 60 °C for 1 h. After incubation, 900 μL of deionized water was added and the absorbance at 562 nm was recorded by an UV-VIS spectrometer (Lambda 45, Perkin Elmer). The standard curve was obtained using native protein.

Fluorescamine assay

A fluorescamine assay was used to determine the number of bound initiators on the protein surface. 40 μL of sample, 100 mM sodium phosphate buffer (40 μL, pH 8), and fluorescamine solution in DMSO (20 μL, 3 mg/mL) were added into a 96-well plate and incubated at room temperature for 15 min. Fluorescence intensities were measured at the excitation of 390 nm and emission of 470 nm with 10-nm bandwidths by a Safire Spike plate reader at the Molecular Biosensor and Imaging Center, Carnegie Mellon University. Initiator concentration was determined using a standard curve using native protein.

Trypsin digestion of protein-initiators Trypsin digestion was performed on protein-initiators to generate peptide fragments to determine modification sites. Peptide fragments were analyzed using matrix-assisted laser desorption/ionization time-of-flight (MALDI-ToF) mass spectrometry. Native CT, CT(N), and CT(+) were digested according to the protocol described in the In-Solution Tryptic Digestion and Guanidination Kit. 20 μg of protein or protein-initiator constructs (10 μL of a 2 mg/mL protein solution in deionized water) were added to 15 μL of 50 mM ammonium bicarbonate with 1.5 μL of 100 mM dithiothreitol (DTT) in an Eppendorf tube. The reaction was incubated for 5 min at 95 °C. 3 μL of 100 mM iodoacetamide aqueous solution was then added and samples were incubated in the dark for 20 minutes at room temperature for thiol alkylation. Next, 1 μL of 100 ng trypsin was added to the tube and the reaction was incubated at 37 °C for 3 hours. Then, an additional 1 μL of 100 ng trypsin was subsequently added. The trypsin digestion was terminated after a total reaction time of 12 hours by the

addition of trifluoroacetic acid (TFA). Digested samples were purified using ZipTipC_{18} microtips and eluted with 2 μL of matrix solution (20 mg/mL sinapinic acid in 50 % acetonitrile with 0.1 % TFA) directly onto a MALDI-ToF plate. The molecular weights of the expected peptide fragments before and after digestion were predicted using PeptideCutter on UniProt P00766 (ExPASy Bioinformatics Portal, Swiss Institute of Bioinformatics). CT-initiator digests were compared to native CT digests. Modification at a particular amino group was determined by either the loss of a peak of the CT-initiator in comparison to native CT or by the appearance of a new peak that equaled the mass (or adducts) of the peptide fragment plus the mass of the initiator (neutral initiator: 220 Da, positive initiator: 320 Da). Fragments below the MALDI-ToF lower m/z=500 limit were not able to be detected.

MALDI-ToF analysis Protein solutions (1.0 mg/mL) were mixed with an equal volume of matrix (Sinapinic acid (20 mg/mL) in 50% acetonitrile with 0.4% trifluoroacetic acid) and 2 μL of the resulting mixture was loaded onto a silver sterling plate target. Apomyoglobin, cytochrome C, and aldolase were used as calibration standards. To determine the extent of initiator modification on protein-initiators, the m/z of the native protein was subtracted from the m/z of the protein-initiator. The difference in m/z was then divided by the mass of the initiator (neutral initiator: 220 Da, positive initiator: 320 Da; after attachment) to obtain the number of initiators per protein. When analyzing trypsin digests of protein-initiators, Bradykinin fragment, angiotensin II (human) and insulin oxidized B chain (bovine) were used as calibration standards. MALDI-ToF data was collected on a PerSeptive Voyager STR MS with nitrogen laser (337 nm) and 20 kV accelerating voltage with a grid voltage of 90 %. 300 laser shots covering the complete spot were accumulated for each spectrum.

Isoelectric Focusing (IEF) gel Criterion IEF precast gels (pH 3-10, 12+2 well, polyacrylamide gel, 13.3 x 8.7 cm) from Bio-Rad were used to determine the isoelectric point of proteins and protein-initiators. Protein solutions (concentration depended on sample) were mixed with 50% glycerol using a 1 to 10 ratio of protein sample to 50% glycerol. 30 μL were loaded into each well. The IEF standards were prepared and loaded according to the Bio-Rad instruction manual. The gel was run in a stepwise manner as follows: 100 V for 60 minutes, 250 V for 60 minutes, 500 V for 30 minutes. Gels were silver stained using the Pierce Silver Stain Kit following their instructions.

Protein-pCBMA and pSMA conjugate synthesis

A solution of monomer (230 mg for CBMA and 246 mg for SMA, 1.0 mmol respectively) and CT-initiator (23 mg for neutral and 25 mg for positive initiator, 10 μmol of initiator) in 100 mM sodium phosphate (20 mL, pH 7) was sealed and bubbled with nitrogen gas in an ice bath for 30 min. 2 mL of deoxygenated catalyst solution (described previously[45]) was added to the polymerization reactor under bubbling nitrogen. The mixture was sealed and stirred in a refrigerator for 1 h. The conjugate was isolated by dialysis with a 25 kDa molecular weight cutoff dialysis tube in deionized water or 25 mM sodium phosphate buffer in a refrigerator for 24 h and then lyophilized. Conjugate CT content was determined by BCA assay as described previously.[32] Other protein-polymer conjugates were prepared using the same ATRP reactant ratios, but at ~5x lower concentration of all reactants, and analyzed by the same procedure as CT-polymers. Monomer concentrations to target DPs of 100 were used for all conjugates except avidin, which was targeted at 150. Monomer conversions are listed in **Table S2**.

Acid hydrolysis and characterization of cleaved polymer

The grafted polymer was cleaved by acid hydrolysis from the conjugate. Protein-polymer conjugate (20 mg) and 6 N HCl aq. (5 mL) were placed in a hydrolysis tube. After three freeze−pump−thaw cycles, the hydrolysis was performed at 110 °C for 24 h *in vacuo*. The cleaved polymer was isolated by dialysis using a 1 kDa molecular weight cut off dialysis tube in deionized water and was then lyophilized. The molecular weight of the cleaved polymer was measured by GPC.

Dynamic light scattering Dynamic light scattering data was collected on a Malvern Zetasizer nano-ZS located in the Department of Chemistry, Carnegie Mellon University, Pittsburgh, PA. The hydrodynamic diameters (number and volume distributions) of samples were measured three times (5 runs per measurement) at room temperature.

Prediction of logD ChemAxon was used to draw the structure of and calculate the hydrophobicity (logD) of lysine side chains and lysine-initiators.

Activity Assays

CT: *N*-succinyl-Ala-Ala-Pro-Phe-*p*-nitroanilide (Suc-AAPF-*p*NA) was used as a substrate for CT. Substrate (0-20 mg/mL in DMSO, 30 μL) was added to a 1.5 mL cuvette with sodium phosphate buffer (pH 8, 100 mM). Native CT, CT-initiators, or CT-polymers (0.1 mg/mL protein, 4 μM, 10 μL) was added to the cuvette with substrate and buffer. The initial substrate hydrolysis rate was measured in triplicate by recording the increase in absorbance at 412 nm over the first 60 seconds after mixing using a Lambda 2 Perkin Elmer ultraviolet-visible spectrometer equipped with a temperature-controlled cell holder at 37 °C. Michaelis-Menten parameters were determined using nonlinear curve fitting of initial hydrolysis rate versus substrate concentration in GraphPad.

Lysozyme: Activities of native, lysozyme-initiator, and polymer conjugates were determined by turbidimetric assays. Lyophilized *Micrococcus lysodeikticus* (Sigma Aldrich) was used to monitor enzymatic catalysis of cell wall lysis. Absorption at 450 nm of suspended *M. lysodeikticus* (990 μL, 0.2 mg/mL) in 50 mM sodium phosphate (pH 6.0) was measured by an UV-VIS spectrometer. 10 μL of native and lysozyme-initiator solutions (1.4 μM in 50 mM sodium phosphate (pH 6.0)) were added and the change of absorbance at 450 nm at room temperature was monitored.

Avidin: HABA is an azo-dye that binds to avidin and shows spectral changes, thus can be used for determination of avidin binding affinity[2]. The absorption at 500 nm of a 200 μM HABA solution in phosphate buffered saline without calcium or magnesium (986 μL, Lonza) was measured using an UV-VIS spectrometer. 16 μL of the conjugate solution (125 μM of avidin in deionized water) was added to the HABA solution and incubated at room temperature for 1 min, and then the absorption at 500 nm was measured. The change in absorbance at 500 nm was used to determine the amount of bound HABA to the conjugate. It has been previously shown that upon biotin binding, tryptophan fluorescence of avidin is decreased from 337 to 324 nm.[3] We detected changes in intrinsic tryptophan fluorescence confirming biotin binding and took biotin binding kinetic measurements using a stopped-flow spectrometer with fluorescence detection (Applied Photophysics SX20). The excitation wavelength was 295 nm with a 5 nm bandwidth. The instrument was permitted to collect 1000 data points throughout the reaction (0.1-450 s). For all experiments, the avidin concentration was 0.5 μM (final) and biotin concentration was 5.0 μM (final). Reactions were initiated by mixing equal volumes of avidin with its substrates in 0.1 M phosphate buffer, pH 8. Fluorescence was measured in volts. Data were fit to single exponential functions using the $F(t) = F_\infty - \Delta F \exp(-k_{obs}t)$ equation, where, k_{obs} is the observed first-

order rate constant, F_∞ is the final value of fluorescence and ΔF is the amplitude. In case of native avidin kinetics, the data were fit to single exponential functions using $F(t) = F_\infty + \Delta F \exp(-k_{obs}t)$, where k_{obs} is the observed first-order rate constant, F_∞ is the final value of fluorescence, and ΔF is the amplitude.

Uricase: Uric acid (0 – 400 μL of 300 μM in 50 mM sodium tetraborate (pH 8.5)) was mixed with 50 mM sodium phosphate buffer (990 – 580 μL, pH 8.5). Native, initiator, and polymer conjugate solutions (10 μL, 20 μM of uricase) were added to the substrate solution. The initial rate was monitored by recording the decreasing in absorbance at 290 nm using an UV-VIS absorbance spectrometer with a temperature controlled cell holder at 37 °C. Michaelis-Menten parameters were determined by nonlinear curve fitting of initial rate versus substrate concentration plots using Prism 7 software (GraphPad).

AChE: Acetylthiocholine iodide (0 – 100 μL of 10 mM in 100 mM sodium phosphate buffer (pH 7.4)) and 10 μL of DTNB solution (50 mM in DMSO) were mixed with 100 mM sodium phosphate (980 – 880 μL, pH 7.4). Native, initiator, and polymer conjugate solutions (10 μL, 4.2 μM of AChE) were added to the substrate solution. The initial rate was monitored by recording the increase in absorbance at 412 nm using an UV-VIS absorbance spectrometer with a temperature controlled cell holder at 37 °C. Michaelis-Menten parameters were determined by nonlinear curve fitting of initial rate versus substrate concentration plots using Prism 7 software (GraphPad).

Residual activity assays

CT: Native CT, CT-initiators, and CT-polymers (1 mg/mL, 40 μM protein) were dissolved in sodium phosphate buffer (pH 8, 100 mM). In triplicate, samples were then diluted to 4 μM for incubation. For thermostability, samples were incubated at 50 °C and pH 8 in a circulating water

bath. For acid stability, samples were incubated at pH 1(167 mM HCl) and 37 °C. At specified time points, aliquots of 10 μL were removed over 60 minutes and residual activity was measured using Suc-AAPF-pNA as a substrate (6 mg/mL, 30 μL, 288 μM in DMSO) in sodium phosphate buffer (pH 8, 100 mM, 37 °C, 960 μL). Initial hydrolysis rate was measured as the increase in absorbance at 412 nm over 40 seconds and data was normalized to its optimal activity (pH 8, 37 °C) at time 0.

***Lysozyme*:** Native lysozyme, initiator, and polymer conjugates (14 μM of lysozyme) in 50 mM sodium phosphate buffer (pH 6.0) were incubated at 80 °C. At given time points, aliquots (10 μL) were removed and activity was measured in 990 μL of suspended *M. lysodeikticus* (0.2 mg/mL) in 50 mM sodium phosphate (pH 6.0) at room temperature. Rates were monitored by recording the decreasing in absorbance at 450 nm using an UV-VIS spectrometer. The residual activity was calculated as a ratio of the initial rates of the reaction at the given time points over the initial activity at time zero.

Uricase: Native uricase, initiator, and polymer conjugates (20 μM of uricase) in 50 mM sodium borate buffer (pH 8.5) were incubated at 75 °C. At given time points, aliquots (10 μL) were removed and activity was measured in 990 μL of 100 μM uric acid in 50 mM sodium borate buffer (pH 8.5) at 37 °C. Rates were monitored by recording the decrease in absorbance at 290 nm using an UV-VIS spectrometer. The residual activity was calculated as a ratio of the initial rates of the reaction at the given time points over the initial activity at time zero.

AChE: Native, initiator, and polymer conjugates (1.4 μM of AChE) in 100 mM sodium phosphate buffer (pH 7.0) were incubated at 50 °C. At given time points, aliquots (10 μL) were removed and added to a mixture of 930 μL of 100 mM sodium phosphate (pH 7.4), 50 μL of acetylthiocholine iodide (10 mM in 100 mM sodium phosphate (pH 7.4) and 10 μL of DTNB

solution (50 mM in DMSO) at 37 °C. Activity rates were monitored by recording the increase in absorbance at 412 nm using an UV-VIS spectrometer. The residual activity was calculated as a ratio of the initial rates of the reaction at the given time point over the initial activity at time zero.

Tryptophan Fluorescence Fluorescence measurements were collected using a BioTek Synergy H1 Plate Reader. Native CT, CT-initiators, and CT-polymers (1 mg/mL, 40 μM protein) were dissolved in sodium phosphate buffer (pH 8, 100 mM). Samples were diluted to 0.1 mg/mL (4 μM protein) in a black round bottom 96 well plate in triplicate. For thermostability, samples were incubated at 45 °C (maximum temperature setting for the BioTek Synergy H1 plate reader) and pH 8. For acid stability, samples were incubated at pH 1 (167 mM HCl) and 37 °C. Fluorescence intensity was measured every 2 minutes over 60 minutes (excitation at 270 nm, emissions at 330 nm and 350 nm). The ratio of emission fluorescence intensities (350 nm/330 nm) was plotted over time with time 0 as the fluorescence intensity of the sample at pH 8 and 37 °C.

Molecular Dynamics Simulation CT-positive initiator model was built with the Maestro Schrodinger build toolkit using the crystal structure of CT as the initial structure (PDB: 4CHA). Positive initiators were attached to the N-terminus and all 14 lysine residues to create a fully modified CT-positive initiator construct. The molecule was subjected to a 1 ns simulated annealing using Desmond. Simulated annealing was performed in 4 stages: linear increasing temperature from 300-400 K over 0-100 ps, constant temperature at 400 K from 100-400 ps, linear decreasing temperature from 400-300 K over 400-700 ps, and constant temperature at 300 K from 700-1000 ps. The simulation system was prepared in Desmond system builder and consisted of OPLS 2005 force field, SPC water model, orthorhombic minimized box, and NaCl ions to neutralize the box followed by the addition of 100 mM NaCl. NVT ensemble and

Berendsen thermostat were used to control temperature with a 1 ps relaxation time. The van der Waals interaction had a cutoff of 9 Å and particle mesh Ewald was used for Coulomb interactions with a 9 Å switching distance. The molecule was simulated using Desmond over 1 ns with a 1.2 ps recording energy interval and 5 ps trajectory recording. A molecular dynamics simulation production run was performed on the final structure from simulated annealing. The simulation was performed over 20 ns at 300 K with a time-step bonded of 2 fs and a NPT ensemble (trajectories were recorded every 1.2 ps and energy was recorded every 4.8 ps). "Nose-Hoover chain" thermostat and "Martyna-Tobia-Klein" Barostat methods were used with 2 ps relaxation time and isotropic coupling. The default relaxation protocol was used with a 9 Å cutoff for van der Waals interactions. The solute atoms were restrained first with a force constant of 50.0 kcal $mol^{-1}Å^{-1}$. Next, the solute heavy atoms were restrained with a force constant of 50.0 kcal $mol^{-1}Å^{-1}$. After the production run, the trajectory was then loaded into Visual Molecular Dynamics (VMD) software for further analysis. The VMD salt bridge plug-in was used to monitor salt bridge formation and location over the 20 ns trajectory caused by initiator-induced structural changes. Salt bridges were monitored between acidic and basic protein residues and not from charges originating from the initiator itself.

Data Availability. All relevant data is included in the manuscript, supporting information, or may be available upon author's request.

RESULTS AND DISCUSSION

Bioconjugate Synthesis and Characterization

We first synthesized a positively charged ATRP-initiator (**Figure S2**). *N*-(3-*N',N'*-Dimethylaminopropyl)-2-bromoisobutyramide and 4-bromobutyryl-*N*-oxysuccinimide ester were synthesized and then reacted with each other to form a positively charged ATRP-initiator. The

overall synthesis had a 68% yield. The positive charge was in the form of a quaternary ammonium, NR_4^+, which was located approximately halfway between the protein-reactive NHS group and the terminal alkyl halide. The positive charge on the initiator quaternary nitrogen atom is therefore extended by 5.6 ± 0.2 Å from the original charge on the lysine NZ atom. We selected a quaternary ammonium group as the source of the positive charge since it would remain positively charged at all pH's and would have a higher propensity of providing stabilization due to its chaotropic cationic nature.

We have previously studied polymer-based protein engineering of the serine protease chymotrypsin. Therefore, we naturally began our exploration of the impact of a permanently positively charged initiator on enzyme structure, dynamics and function by measuring the kinetics and stability of chymotrypsin-initiator constructs and chymotrypsin-polymer conjugates. Our previous studies have shown that chymotrypsin loses activity but gains stability when poly(carboxybetaine methacrylate) (pCBMA) is grown from the surface. Conversely, poly(sulfonate methacrylate) (pSMA) rapidly destroys the function of chymotrypsin (**Scheme 1**).[9,32]

Scheme 1. Synthetic approach to prepare grafted-from protein-polymer conjugates using neutral (N) or positively charged (+) initiators. The initiators reacted with primary amino groups on the protein surface through NHS chemistry. ATRP was then performed from the bio-macroinitiators using a zwitterionic polymer, pCBMA, or a negatively charged polymer, pSMA.

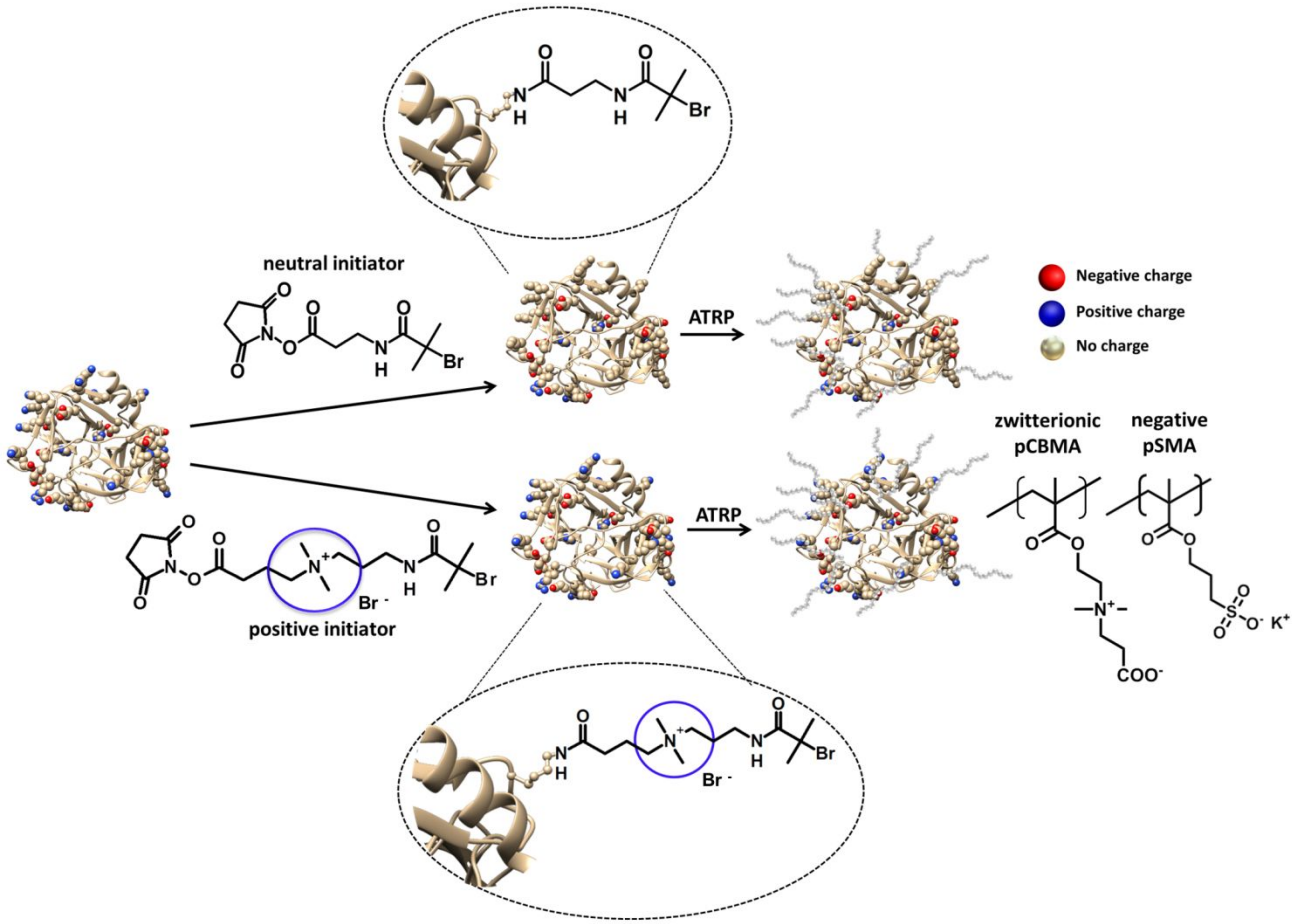

The CT-initiator constructs were analyzed with matrix assisted laser desorption/ionization time-of-flight (MALDI-ToF) mass spectroscopy to determine the average number of amino groups that had been modified (**Figure S6**). CT has 15 total amino groups (N-terminus and 14 lysines). The average numbers of initiators attached to CT were 14.1 and 10.6 for the neutral (N) and positively charged (+) initiators, respectively (**Table 1**). The slight decrease in total number of positive initiator modifications in comparison to the neutral initiator was likely due to its larger size and charge. The larger size could inhibit reactions with primary amines that have decreased accessible surface areas while the positive charge could hinder reactions with primary amines in positively charged regions of CT.[50] In order to determine the

sites of modification for each protein-initiator constructs, trypsin digestion followed by analysis of peptide fragments using MALDI-ToF was performed (**Figure S7 and Tables S3 and S4**).[50] The same sites were modified with the neutral and positively charged initiators except K82, K84, K90, K177, and K202. In general, these sites had decreased exposed surface areas which made them unable to be modified by the positively charged initiator, which was larger in size than the neutral initiator.[50] We were first interested in determining how the different CT-initiators impacted the isoelectric point (pI) of CT, which is the pH at which CT has no net electrical charge. We used isoelectric focusing (IEF) gel electrophoresis with a pH 3-10 gradient (**Figure S8**) to study the protein charge in the enzyme-initiator constructs. Native CT has a pI of approximately 8.75.[54] The pI of the CT(N) construct dropped to pI values ranging from ~3-6, with the majority of the band intensity at the limit of the gel around pH 3. There were three distinct bands: pI ~3, 5, and 6 which were most likely due to sub-populations of protein-initiators that had different numbers of reacted initiators. While MALDI-ToF provided an average number of modifications in the sample, the IEF gel allowed us to visualize the sub-populations with different degrees of modification. The decrease in pI for CT(N) was expected since the protein was losing positive charges and becoming more acidic. The pI values for CT(+) were increased to ~5-7.5 from CT(N), but were still decreased from native CT. pI values arise from an average of the individual residue pK_a values, which are highly sensitive to their local electrostatic environment.[55] It is also known that charge-charge interactions are the dominant factor that shift pK_a values of ionizable groups on the protein surface.[56] Since our positively charged initiator did not have a pK_a, it made sense that the pI of CT(+) would be restored to intermediate values relative to native CT. After verifying that pI values for CT(+) were increased to ~5-7.5 from

CT(N), protein-polymer conjugates were synthesized with incompatible (pSMA) and compatible (pCBMA) polymers (**Table 1**).

Table 1. Characterization and activities of native CT, CT-initiators, and CT-polymers.

		Number of initiators	Cleaved polymer M_n (kDa); PDI	Conjugate M_n *(kDa);DP	D_h (nm) Number Dist.	Turnover number, k_{cat} (s^{-1})	Michaelis Constant, K_M (μM)	Catalytic Efficiency, k_{cat}/K_M ($\mu M^{-1}s^{-1}$)
Chymotrypsin	**Native**	--	--	--	3.98 ± 0.48	26.6 ± 0.3	107 ± 5	0.25 ± 0.01
	(+)	10.6	--	--	4.18 ± 0.70	21.6 ± 0.6	60 ± 7	0.36 ± 0.03
	(N)	14.1	--	--	4.07 ± 0.31	18.9 ± 0.4	53 ± 5	0.36 ± 0.03
	(+)-pSMA	10.6	21.7; 1.44	256: 82	14.3 ± 7.5	22.2 ± 0.2	109 ± 3	0.20 ± 0.004
	(N)-pSMA	14.1	19.9; 1.54	306; 75	12.9 ± 6.9	3.0 ± 0.2	217 ± 35	0.01 ± 0.002
	(+)-pCBMA	10.6	23.8; 1.57	278; 104	18.3 ± 3.4	30.5 ± 0.6	73 ± 6	0.42 ± 0.02
	(N)-pCBMA	14.1	18.1; 1.54	281; 79	17.5 ± 7.7	25.6 ± 0.2	84 ± 3	0.30 ± 0.01

* Conjugate M_n=(cleaved polymer M_n × number of initiators) + molar mass of CT.

The molecular weights of the polymers were kept constant (targeted degree of polymerization of 100) in order to compare the activity and stability of each conjugate to that of the native enzyme.[57] After ATRP and purification of the conjugates via dialysis, protein-polymer conjugates were characterized with a bicinchoninic acid (BCA) assay to determine protein concentration from which conjugate molecular weight and degree of polymerization were estimated.[10] The polymers were also cleaved from the protein surface via acid hydrolysis and the isolated polymers were analyzed by gel permeation chromatography for relative molecular weight and polydispersity (PDI) from which conjugate molecular weight and degree of polymerization were also calculated. Conjugate number-average molecular weights reported in **Table 1** are derived from GPC data, however, BCA and GPC results agreed well. Number average hydrodynamic diameters (D_h) were also measured using dynamic light scattering and conjugates grew in size from 3.98 nm for native CT to approximately 13 nm for CT-pSMA and

approximately 18 nm for CT-pCBMA conjugates grown from either CT(+) or CT(N). CT-pCBMA conjugates had slightly larger hydrodynamic diameters because pCBMA is super-hydrophilic which would give CT-pCBMA a larger hydration layer than CT-pSMA conjugates. Only single peaks were detected in DLS by number and volume distributions (**Figures S9-S12**) and there were no signs of visible aggregation.

Impact of charged initiator on activity of an incompatible protein-polymer conjugate

Attachment of polymers to proteins usually causes significant activity reductions, which have been attributed to protein structural stiffening.[58] The degree of protein modification and activity loss are also tightly correlated. Negatively charged polymers, such as pSMA, have been previously shown to inactivate CT rapidly.[32] Indeed, in the previous study, tryptophan fluorescence intensity at pH 8.0 increased after the CT(N)-pSMA conjugate was synthesized, indicating that the conjugate was already partially unfolded even in its most optimal environment.[32] We next explored whether maintaining enzyme surface charge, using a charged initiator, could protect the biocatalytic activity in CT-pSMA conjugates. Activities were measured by Michaelis-Menten kinetics at pH 8 and 37 °C using Succinyl-Ala-Ala-Pro-Phe-*p*-nitroanilide (Suc-AAPF-*p*NA), a hydrophobic and negatively charged substrate for CT, that binds to the hydrophobic S_1 binding pocket and is then cleaved by the catalytic triad (Ser 195, His 57, Asp 102). The turnover numbers (k_{cat}, s^{-1}), Michaelis constants (K_M, μM), and overall catalytic efficiencies (k_{cat}/K_M, $\mu M^{-1}s^{-1}$) were first determined for native CT and CT-pSMA conjugates grown from either neutral or positive initiators (**Table 1**). The growth of pSMA from CT(N) caused CT to lose 97% of its activity, matching results from previous work.[9,32] Unfortunately, this degree of activity loss is not unprecedented for protein-polymer conjugates in

general. We were delighted to observe that the CT(+)-pSMA conjugate showed similar activities to native CT in terms of both k_{cat} and K_M. It is important to note that the positively charged initiator modified less sites than the neutral initiator (10.6 vs. 14.1). In our prior work with chymotrypsin, however, we have shown that the activities of CT modified at 11 sites and 13 sites were similar[51], so we believe that the activity difference between the neutral and positively charged initiator was related to charge versus number of modifications.

We next considered *why* a simple charged initiator might have such a profound effect on protein surface electrostatics when surrounded by a vast array of negative charges in the polymer. After all, the CT(+)-pSMA conjugate retained 10 positive charges at its surface, but added over 1,000 negative charges to the molecular shell. Charged groups produce an electric field due to interactions with other charged particles in close proximity. The electric field strength at a surface with propagating point charges can be estimated using (equation 2),

$$E = \frac{kq}{r^2} \quad (2)$$

where E is electric field (NC^{-1}), k is Coulomb's constant (9.0E9 Nm^2C^{-2}), q is the signed magnitude of the point charge, and r is the distance between the charges. Therefore, the electric field strength is proportional to the magnitude of the electric charge and inversely proportional to the squared distance. A CT(+)-pSMA conjugate of one polymer chain was modeled to estimate the electric field strength at the protein surface (**Figure 1**). Since the electric field is additive, even if there were 100 negative charges (DP=100) following the positive charge, the electric field strength at the protein surface would still be +0.77. This calculation assumes that the polymer backbone is in a linear conformation, which might not be true for all polymer types, but we have previously shown through molecular dynamics simulation that pSMA is a rather stiff, inflexible polymer, increasing the validity of the assumption.[32] This informative example

highlights the importance of maintaining optimal surface charge prior to growth of charged polymers. Since the positively charged initiator was able to maintain high levels of activity of an incompatible polymer-protein conjugate, we next explored whether it may also improve conjugate stability when exposed to typical stressors, such as temperature and pH.

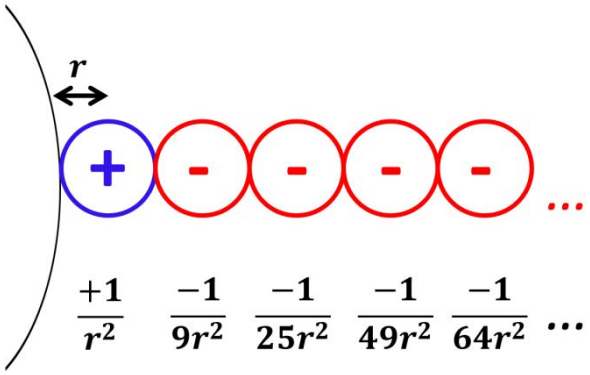

Figure 1. CT(+)-pSMA conjugate modeled as point charges. The positive charge is from the quarternary ammonium on the positive initiator while the remaining negative charges are the anionic sulfonate groups on SMA monomers. Even if there were 100 negative charges to the right of the positive charge, the electric field strength at the protein surface would still be +0.77.

Impact of charged initiator on stability of an incompatible protein-polymer conjugate

Various strategies have been used to stabilize protein solutions including adding excipients (polyols and salts)[36,59,60], immobilization onto solid supports,[61] encapsulation into reverse micelles[62], or by covalent attachment of polymer.[9] CT has a two-step deactivation mechanism where it undergoes complete deactivation via an intermediate transition state as follows (**1**),[63]

$$F \overset{k_1}{\leftrightarrow} I \overset{k_2}{\rightarrow} U \qquad (1)$$

where F, I, and U are the folded, intermediate, and unfolded conformational states, and k_1 and k_2 are first order deactivation rate constants (min^{-1}). CT, when conjugated with polymer, resists inactivation by either not unfolding or refolding at a high rate.[63] We first determined the resistance of CT-pSMA conjugates to inactivation by heat (50 °C, pH 8) and acid (pH 1, 37 °C)

(**Figure 2**). Deactivation via temperature and pH were chosen because they are two common stressors for protein structural stability and are valuable parameters for both industrial and therapeutic applications of enzymes. Covalently attached polymers have the ability to increase the temperature and pH working ranges of the enzyme to increase their robustness during industrial processing. At specified time points, aliquots were taken from the incubating samples and activities were measured at pH 8 and 37 °C. CT(N)-pSMA irreversibly inactivated after just 10 minutes at 50 °C (**Figure 2A**). In another demonstration of the impact of the positive initiator, CT(+)-pSMA was remarkably stable as it retained 60% residual activity at 60 minutes. Our prior work has elucidated the mechanism of CT-polymer conjugate resistance to acid induced irreversible inactivation where the polymers trap proteins in partially unfolded intermediate states, prevent complete unfolding, and assist in refolding.[32] In acid, CT(+)-pSMA also displayed higher stability and was able to maintain 20% residual activity in comparison to CT(N)-pSMA, which had immediately irreversibly inactivated (**Figure 2B**). These data, in combination with Michaelis-Menten activity data, were the first observations to our knowledge of both high activity and stability with a negatively charged protein-polymer conjugate. The stability data further confirmed our view of the importance of net protein surface charge restoration when growing polymers from protein surfaces. Next, we began to dissect the interactions between the protein surface and the bio-macroinitiators.

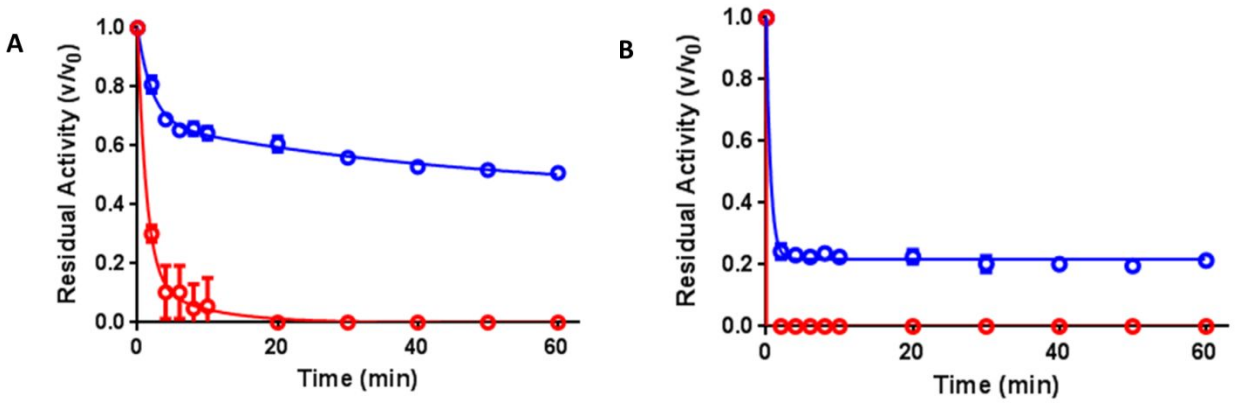

Figure 2. A) CT-pSMA thermal stabilities at 50 °C and pH 8 and **B)** CT-pSMA acid stabilities at pH 1and 37 °C for conjugates grown from (N) or (+) initiators. CT(N)-pSMA (○), and CT(+)-pSMA (○). CT-pSMA conjugates synthesized using the positive initiator had increased thermal and acid stabilities in comparison to their neutral initiator conjugate counterparts. Residual activities were normalized to activity at time 0 which was the conjugate's optimal conditions for activity at pH 8 and 37 °C. Error bars in all plots represent the standard error of the mean from triplicate measurements.

Impact of charged initiator on activities and stabilities of protein-initiator constructs

Michaelis-Menten activities for CT-initiators were measured and are listed in **Table 1**. CT(N) and CT(+) had similar activities, but both had higher overall catalytic efficiencies than native CT due to a decrease in K_M. The observed decrease in K_M upon neutral initiator attachment could have been the result of the hydrophobicity of the initiator. The octanol-water distribution coefficient (log D), which takes into account the hydrophobicity of different ionization states of a charged molecule, of a lysine side chain at pH 8.0 was -1.00 using ChemAxon. After covalent attachment of the neutral initiator, the calculated log D value of a lysine-initiator construct rose to 1.82. Considering that this reaction occurred on 14 out of the possible 15 amino groups, the surface of CT would have undoubtedly become more hydrophobic which would have strengthened the van der Waals interactions between the hydrophobic substrate and hydrophobic S_1 binding pocket to increase the affinity for the substrate. After attachment of the positive initiator, however, the calculated log D of the lysine-initiator construct decreased to -1.98. The

positive charge in the initiator likely maintained favorable electrostatic interactions with the negatively charged substrate to increase the binding affinity.

Since activities were comparable between CT(+) and CT(N), thermal and acid stabilities were probed next. Residual activities were further correlated with conformational tertiary changes by following increases in tryptophan fluorescence emissions over time during incubation at high temperature (45 °C, pH 8). CT(N) had irreversibly inactivated at elevated temperature (**Figure 3A**) and also at low pH (**Figure 3C**) within the first couple minutes. These profiles were drastically different than native CT which slowly deactivated over time. We were pleased to observed CT(+) had a similar thermal stability profile as native CT. When the data were fitted to the two-step inactivation model described by equation 1 using GraphPad's 2-phase decay, CT(+) displayed a larger k_1 and a smaller k_2 than the native enzyme (**Table S5**). At elevated temperature, fluorescence intensity increased substantially over 60 min for CT(N) indicating protein unfolding and exposure of buried aromatic residues while CT(+) and native CT slightly increased to similar degrees, matching the residual activity profiles (**Figure 3B**).[64] In acid, both CT(N) and CT(+) irreversibly inactivated within the first 5 minutes by unfolding as seen in the tryptophan fluorescence immediate increases in intensities (**Figure 3D and Table S6**). Deactivation by heat is due to the breakage of hydrogen bonds with surface residues leading to disorder in the water molecule network around the protein allowing for increased vibrational dynamics and unfolding. Deactivation by pH, however, is due to disruption of the ionizable residues and electrostatic interactions on the protein surface which eventually leads to unfolding. Since modifying amino groups with the ATRP initiators changes the protein's ionizability and the positive initiator creates a non-ionizable positive charge, it was not surprising that unfolding was observed for both CT(N) and CT(+) in acid.

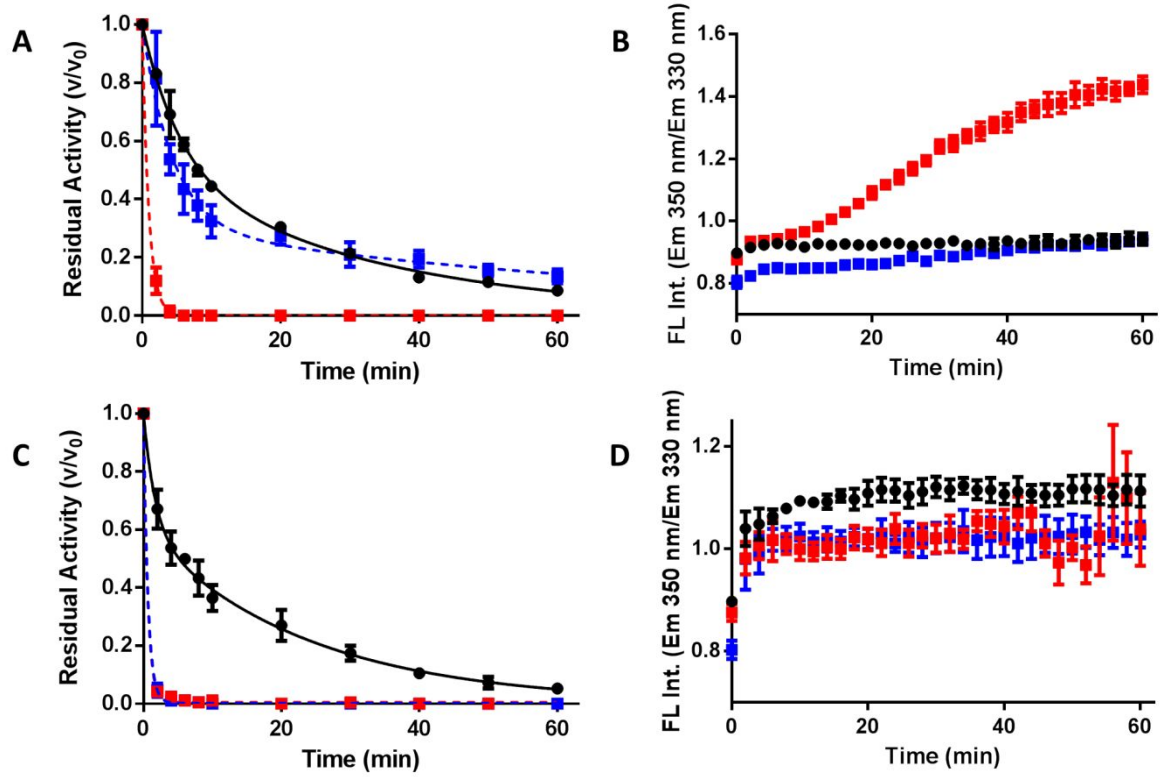

Figure 3. Thermal and acid stabilities of native CT and CT-initiators. Stabilities are normalized to time 0 which represents the most active form of CT (pH 8 and 37 °C). **A)** Residual activities at 50 °C and pH 8 and **B)** tryptophan fluorescence emission intensities at 45 °C and pH 8. Increases in fluorescence intensities indicate protein unfolding as buried aromatic residues become more exposed to the solvent. **C)** Residual activities and **D)** tryptophan fluorescence emission intensities at pH 1 and 37 °C. In all plots, native CT (●), CT(N) (■), and CT(+) (■). Connecting lines are nonlinear fits using GraphPad. At elevated temperature, the CT(N) lost all detectable activity within the first 5 minutes which correlated to rapid unfolding in the tryptophan fluorescence plot. CT(+) displayed similar residual activities and conformational stabilities to native CT indicating that surface charge is important for maintaining CT's stability. In acid, both CT(N) and CT(+) rapidly lost activity as confirmed with rapid unfolding via tryptophan fluorescence. Error bars in all plots represent the standard error of the mean from triplicate measurements.

Next, we were interested if the increased thermal stability of CT(+) was due to altered short range (salt-bridge) or restoration of long range electrostatic interactions. We synthesized a CT-initiator construct that contained a random mixture of neutral and positive initiators around the protein surface. If a specific short-range interaction was causing the stabilization, then random mixed modification should eliminate the possibility of that interaction occurring and the thermal stability of the mixed sample would be similar to that of the neutral initiated sample. Characterization through MALDI-ToF showed that the mixed constructs contained an average of

9 neutral and 5 positive initiators per CT (**Figure S13**). For activity, the mixed construct had slightly lower Michaelis-Menten parameters than both CT(N) and CT(+) (k_{cat}= 16.7 ± 0.4 s^{-1}, K_M= 82 ± 7 μM, k_{cat}/K_M= 0.20 ± 0.01 $\mu M^{-1}s^{-1}$) at pH 8 and 37 °C. For thermal stability at pH 8 and 50 °C, the mixed initiator construct had a stability curve that fell between CT(N) and CT(+) stability curves (**Figure S14)** while the deactivation rate of the CT-mixed initiator (0.55 ± 0.03 min^{-1}) was approximately half of CT(N) (1.06 ± 0.03 min^{-1}). These data implied that the stabilizing effect against heat-induced irreversible inactivation of the positive initiator construct was most likely due to maintenance of long-range surface charge electrostatic interactions versus specific short-range interactions.

To verify that the stabilizing effects were due to long-range electrostatic interactions over short-range (salt bridges), we performed a 20 ns all-atom molecular dynamics (MD) simulation in a water box with periodic boundary conditions on a fully modified CT (PDB: 4CHA) with positive initiators. The simulation was performed to mimic experimental conditions by adjusting the protonation states of ionizable groups to pH 8 and adding 100 mM NaCl. The system was subjected to a 1 ns simulated annealing to place the molecule in its lowest energy state and remove bias in initiator configuration before starting the 20 ns production run. MD simulations were performed using the OPLS2005 force field and the average radius of gyration was 1.85 nm which was validated against experimental hydrodynamic diameter data (**Figure S15**). Electrostatic interactions around the protein surface were monitored over the 20 ns trajectory by determining the number of salt bridge formations, which represent the short-range electrostatic interactions. Salt bridge formation was monitored using Visual Molecular Dynamics (VMD) software plugins. A salt bridge is formed when the distance between any of the oxygen atoms of acidic residues (Asp, Glu) are within 3.2 Å of the nitrogens of basic residues (Arg, His, Lys,

Hsp). Therefore, salt bridges were determined for the lysine portions of lysine-initiator moieties and induced tertiary structural changes to remaining acidic and basic residues, but not for the additional nitrogens on the initiator structure. Native CT has one known salt bridge (between the α-ammonium ion of Ile 16 and the carboxylate ion of Asp 194) and was chosen as the protein for comparison.[65] It was previously found that destabilization of this salt bridge decreased stability by 2.9 kcal mol^{-1}.[65] In the CT-positive initiator construct, we observed the formation of 4 different salt bridges throughout the 20 ns analysis: Asp 72-Arg 154, Glu 21-Arg 154, Asp 129-Arg 230, and Asp 128-Lys203 (**Figure S16A**). Arg 154 is located within close proximity of two acidic residues, Asp 72 and Glu 21, and formed salt bridges with both in the simulated model. The time spent in a salt bridge was also monitored over 20 ns (**Figure S16B**). The most dominant salt bridge was between Asp 72-Arg 154. Since there was only one salt bridge formed that was associated with the lysine portion of a modified lysine residue, it was possible that CT(N) could also form the majority of the salt bridges induced by conformational dynamics. Additionally, the stabilities (residual activities) of CT and CT(+) were similar indicating that the formation of additional salt bridges did not significantly enhance CT's stability. Rather, it was more likely that the maintained stability of CT(+) over CT(N) was due to long-range electrostatic interactions through restoring the charge balance, aligning with the findings of activity and stability of CT-mixed initiator.

Impact of charged initiator on activity and stability of a compatible protein-polymer conjugate

Since the positive initiator generated a highly active and stable conjugate with an "incompatible" polymer, we hypothesized that maintaining natural surface charge may also be able to further

improve the activity and stability of a highly compatible polymer, namely zwitterionic polymer, pCBMA. As stated above, almost all protein-polymer conjugates lose activity to some degree. We were curious whether maintaining surface charge would remove this limitation, or even unusually enhance conjugate function further. We have shown previously[32] that CT-pCBMA conjugates grown from neutral initiators are highly effective (with slightly improved k_{cat}/K_M relative to the native enzyme[66]) (**Table 1**). When using the positive initiator, CT(+)-pCBMA had an increased k_{cat}/K_M (0.30 ± 0.01 to 0.42 ± 0.02 $\mu M^{-1}s^{-1}$) with increased k_{cat} and decreased K_M compared to CT(N)-pCBMA. We also observed that the overall catalytic efficiency of CT(+)-pCBMA was almost double that of native CT. The thermal stability of the CT(+)-pCBMA was also improved relative to native and neutral-initiated conjugate (even maintaining ~90% activity after exposure to high temperature for 60 minutes) (**Figure 4**). Although zwitterionic polymers are now setting the benchmark for modified protein stabilization[35,67,68], this "gold standard" can now be further improved with the use of a positively charged initiator.

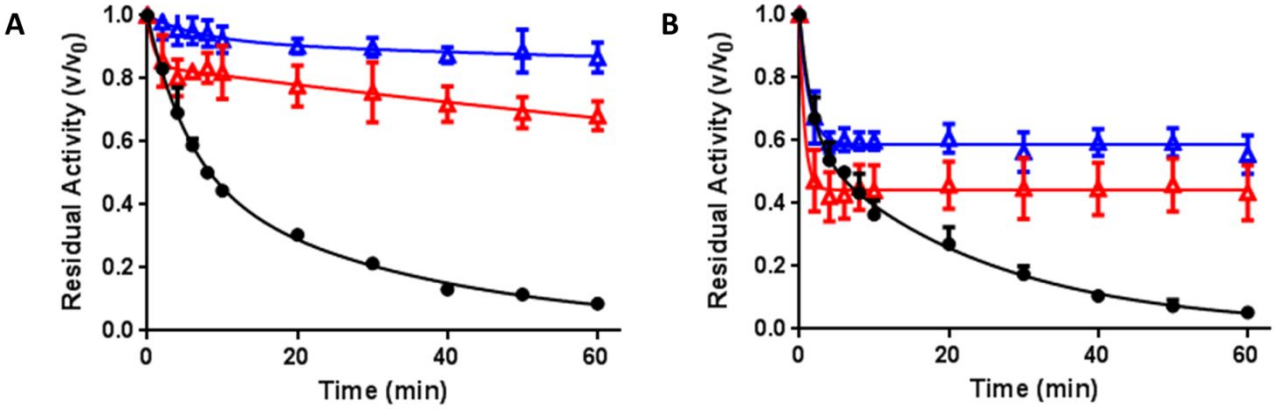

Figure 4. A) CT-pCBMA thermal stabilities at 50 °C and pH 8 and **B)** CT-pCBMA acid stabilities at pH 1and 37 °C for conjugates grown from (N) or (+) initiators. In both plots, CT(N)-pCBMA (▲) , CT(+)-pCBMA (△), and native CT (●). Conjugates synthesized using the positive initiator had increased thermal and acid stabilities in comparison to their neutral initiator conjugate counterparts. Residual activities were normalized to activity at time 0 which was the conjugate's optimal conditions for activity at pH 8 and 37 °C. Error bars in all plots represent the standard error of the mean from triplicate measurements.

Impact of charged initiator on activity and stability of diverse protein-pCBMA conjugates

Since we discovered that the positively charged initiator could generate protein-polymer conjugates with significantly higher activities and stabilities than native chymotrypsin and neutral-initiated chymotrypsin, we decided to explore whether a diverse group of enzymes would also benefit from a positively charged initiator. To make this more challenging, we selected a group of enzymes that are not all ideally suited to polymer-based protein engineering. We modified lysozyme (14.3 kDa, 7 amines), avidin (16.4 kDa, 10 amines), uricase (35 kDa, 25 amines), and acetylcholinesterase (70 kDa, 26 amines) with pCBMA grown from neutral and positively charged initiators. These enzymes have very different molecular weights, number of amino groups, active site mechanisms, multimeric characteristics (molecular weights and number of amines listed are per monomer), and susceptibilities to modification. The degree of initiator modification for each protein-initiator construct was determined using a fluorescamine assay, except for lysozyme and avidin samples, which were characterized by MALDI-ToF (**Figures S17 and S18**). Polymers of CBMA were grown from each of the protein-initiator constructs with similar degrees of polymerization. After synthesis, conjugate molecular weights were estimated by the cleaved polymer molecular weight by GPC.

Activity

The reaction rates and attachment locations of neutral ATRP initiators with lysozyme, a small, single sub-unit protein that is an antimicrobial enzyme and is important for the immune system, have been dissected in detail.[50] Lysozyme hydrolyzes the β-1,4 glycosidic linkages between N-acetylmuramic acid and N-acetylglucosamine that are present in the cell wall of the bacteria. As seen with CT, the degree of initiator modification was slightly less for the positive initiator compared to the neutral initiator (4.6 versus 6.7) (**Table 2**). Lysozyme activity was

measured by the change in absorbance at 450 nm over time when using *Micrococcus lysodeikticus* as a substrate. Lysozyme(N) was almost completely inactive (two orders of magnitude less activity than native lysozyme). The compelling results with CT were mirrored for lysozyme(+) and we observed almost complete restoration of activity for the positively charged protein-initiator construct compared to native. Growth of pCBMA from lysozyme(N) regained activity lost upon neutral initiator attachment while growth of pCBMA from lysozyme(+) only showed moderate further increase in activity. Lysozyme(+)-pCBMA had double the activity of lysozyme(N)-pCBMA.

Avidin, a tetrameric protein (homo-tetramer) that is approximately 66 kDa in its tetrameric form and is found in the egg whites of birds, reptiles, and amphibians, was also modified by the positive initiator to a reduced amount (7.0 versus 7.9). Using a model system we have described previously[69], we determined that the conjugate with the positive initiator had an increased biotin binding rate and increased equilibrium HABA binding over the conjugate with the neutral initiator (**Table 2**).

In the liver, uricase catalyzes the oxidation of uric acid by gaseous molecular oxygen to produce 5-hydroxyisourate and hydrogen peroxide.[70,71] Uricase has a homo-tetrameric structure and the active sites of the monomers are located at dimeric interfaces. There is also a hydrophobic cavity on each monomer located next to its active site and the flexibility of this cavity is essential for catalysis.[72] The therapeutic utility of uricase makes it an ideal target for polymer-based protein engineering, but the enzyme has been found to lose almost all activity upon polymer modification when densely modified. As expected, uricase(N) was largely inactivated and very little activity was detectable. The loss in activity was due to a combined decrease in k_{cat} and increase in K_M compared to native. Surprisingly, growth of pCBMA did not

recover the lost activity of uricase(N) and in fact, caused complete inactivation of uricase(N)-pCBMA. Initiation of uricase with the positively charged initiator resulted in an enzyme with detectable activity, though the activity was still significantly less than the native enzyme due to high modification. Growth of pCBMA from uricase(+) also yielded a protein-polymer conjugate with detectable activity. The large decrease in activity could be due to a combination of decreased flexibility (causing decreased k_{cat}), modification of Lys 10 in the active site (causing inactivation), increased hydrophilicity of the cavity when using the positive initiator (causing increased K_M), or loss of tetrameric structure due to high modification densities. We are now optimizing uricase activity by targeting each of these issues.

Acetylcholinesterase (AChE) catalyzes the hydrolysis of acetylcholine to acetic acid and choline. The positively charged substrate binds to the anionic site of AChE and is then hydrolyzed by the catalytic triad (Ser 200, Glu 327, His 440).[73,74] AChE(N)-pCBMA had decreased activity over both AChE and AChE(N), due largely to a decrease in k_{cat}. Once again, however, the positively charged initiator-grown protein-polymer conjugate (AChE(+)-pCBMA) did not show any further activity loss after the growth of polymer.

Table 2. Characterizations and activities of a range of proteins and their subsequent protein-initiators, and protein-polymers. Conjugate data are calculated per monomer. Errors on activity data are calculated from standard deviations of triplicate measurements. U.D. stands for undetectable in cases where conjugation fully inactivated the protein.

		Number of initiators	Cleaved polymer M_n (kDa); PDI	Conjugate M_n (kDa)	D_h (nm)	Activity		
						ΔA_{450} x10^{-4} (s^{-1})		
Lysozyme	Native	--	--	--	2.6 ± 0.9	32.3 ± 0.5		
	(N)	6.7	--	--	2.8 ± 1.0	1.0 ± 0.1		
	(+)	4.6	--	--	2.9 ± 1.0	23.7 ± 1.5		
	(N)-pCBMA	6.7	9.4; 1.38	77.0	9.5 ± 1.6	10.2 ± 0.2		
	(+)-pCBMA	4.6	9.2; 1.34	56.3	8.6 ± 1.0	28.5 ± 0.4		

						Biotin binding rate (s^{-1})	HABA binding, K_{assoc} (μM)	
Avidin	**Native**	--	--	--	5.8 ± 0.5	92.5 ± 14.1	2.13 ± 0.09	
	(N)	7.9	--	--	5.6 ± 0.6	1.09 ± 0.07	2.10 ± 0.12	
	(+)	7.0	--	--	6.3 ± 1.8	1.69 ± 0.04	2.11 ± 0.10	
	(N)-pCBMA	7.9	27.9; 1.82	237.4	26.8 ± 2.5	0.23 ± 0.07	0.56 ± 0.01	
	(+)-pCBMA	7.0	32.0; 1.93	241.0	26.9 ± 3.4	1.64 ± 0.08	0.71 ± 0.01	
						Turnover Number k_{cat} (s^{-1})	**Michaelis Constant K_M (μM)**	**Catalytic Efficiency k_{cat}/K_M ($\mu M^{-1}s^{-1}$)**
Uricase	**Native**	--	--	--	7.3 ± 3.0	3.42 ± 0.05	12.9 ± 0.6	0.266 ± 0.013
	(N)	25.3	--	--	8.5 ± 2.5	0.18 ± 0.01	119.4 ± 9.7	0.002 ± 0.0006
	(+)	19.8	--	--	8.7 ± 2.0	2.14 ± 0.04	25.4 ± 1.4	0.084 ± 0.005
	(N)-pCBMA	25.3	8.8: 1.41	257.6	16.1 ± 5.1	U.D.	U.D.	U.D.
	(+)-pCBMA	19.8	8.1: 1.36	195.4	17.3 ± 8.9	0.03 ± 0.003	22.0 ± 7.6	0.001 ± 0.0005
Acetylcholinesterase	**Native**	--	--	--	8.6 ± 1.8	120.5 ± 3.3	309 ± 21	0.390 ± 0.029
	(N)	14.2	--	--	9.2 ± 2.7	98.6 ± 1.9	206 ± 12	0.479 ± 0.029
	(+)	10.2	--	--	9.4 ± 2.1	119.1 ± 2.7	337 ± 19	0.353 ± 0.021
	(N)-pCBMA	14.2	7.9; 1.35	184.0	12.3 ± 2.4	2.9 ± 0.1	275 ± 19	0.010 ± 0.007
	(+)-pCBMA	10.2	8.5; 1.34	158.5	11.9 ± 2.6	115.0 ± 3.2	329 ± 22	0.349 ± 0.026

Stability

The rates of heat-induced irreversible inactivation of lysozyme-initiators and subsequent lysozyme-polymer conjugates were assessed by measuring residual activities over time during incubation at 80 °C (**Figure 5A**). Lysozyme(N) had the lowest thermal stability and had lost approximately 60% of its original activity after 2 minutes at 80 °C. The stability of lysozyme(N) was regained upon growth of pCBMA and was similar to those of native, lysozyme(+), and lysozyme(+)-pCBMA. The rates of heat-induced irreversible inactivation of uricases were determined by measuring the residual activities over time at 75 °C. Uricase(N) stability was

decreased in comparison to native uricase while uricase(+) was higher than native uricase (**Figure 5B**). Uricase(+)-pCBMA had a similar thermal stability as uricase(+). The rates of heat-induced irreversible inactivation of acetylcholinesterases were determined next by measuring the residual activities over time at 50 °C (**Figure 5C**). AChE(N) was irreversibly inactivated within the first 2 minutes of incubation at 50 °C. Stability was regained after growth of pCBMA from AChE(N) and was comparable to the native enzyme. AChE(+) showed increased thermal stabilities over AChE(N) and was also comparable to native AChE. Conjugates of AChE(+)-pCBMA showed the highest thermal stabilities of all AChE samples retaining approximately 70% activity after 60 minutes of incubation at elevated temperatures.

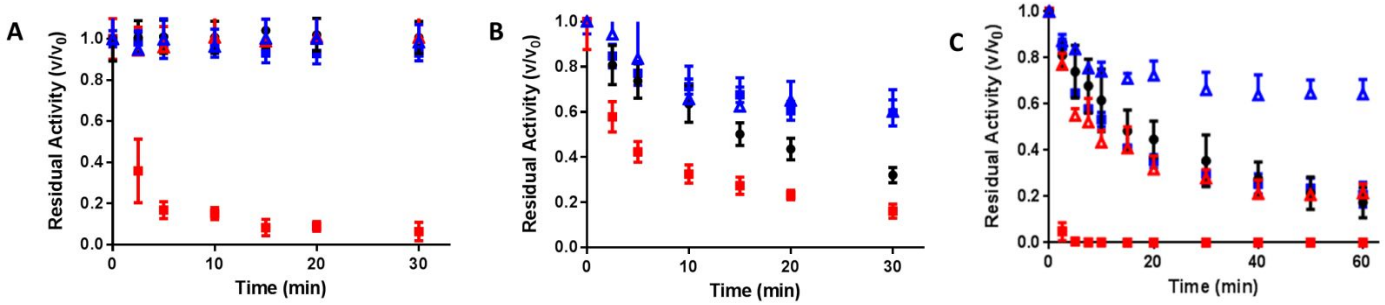

Figure 5. Thermal stabilities for grafted-from **A)** lysozyme samples (80 °C), **B)** uricase samples (75 °C), and **C)** acetylcholinesterase samples (50 °C) as residual activities over time normalized to activities at time 0. In all plots, native protein (●), protein(N) (■), protein(+) (■), protein(N)-pCBMA (△), and protein(+)-pCBMA (△). In general, samples prepared with the positive initiator had higher thermostabilities over their neutral counterparts. Error bars represent standard deviations from triplicate measurements.

Conclusions

Overall, conjugates grown from the positively charged bio-macroinitiator constructs all showed increased activities in comparison to their neutral bio-macroinitiator construct counterparts. All of the protein(+)-polymer conjugates also had increased thermostabilities in

comparison to the protein(N)-polymer conjugates. As we had observed for CT, the stability curves of the protein(+) constructs were similar to, or better than, those for the native proteins.

Protein-polymer conjugate structure-function-dynamic relationships are important to understand in order to help guide future functional conjugate design. We have shown herein that the use of charged ATRP-initiators that restore surface charge close to native values is crucial to maximizing activity and stability. Moreover, we are now able to safely grow incompatible homopolymers without deactivation or loss in stability, as demonstrated with CT. This can have many far-reaching implications. For example, many biomolecules have negatively charged surfaces/membranes. Having a therapeutic molecule coated with negatively charged polymers would increase repulsive electrostatic forces between these molecules to prevent unwanted interactions or uptake *in vivo*. Supramolecular assemblies could also be created using a bottom-up approach to fabricate higher ordered, reversible structures based on electrostatic interactions with negatively charged polymer conjugates. Additionally, negatively charged polymers containing carboxylic acids that are conjugated to biomolecules could be functionalized to attach drugs or targeting ligands using common carboxylic acid chemistries. Finally, conjugates that are highly negatively charged could increase the efficiency of purification and separation techniques that rely on electrostatic interactions such as ion-exchange chromatography. The idea of using a charge-maintaining initiator can further be generalized for other conjugation strategies. For example, when targeting residues that have negatively charged carboxylic acids, a negatively charged initiator might be beneficial. Additionally, the initiator structure can be designed in such a way that it places the charged group at a desired distance from the protein surface, which could tune activity. Taking inspiration from this work, we are now exploring the impact of amine-targeting positive charge retaining “grafting-to” strategies as a way to restore the activity of

PEGylated proteins. Maintenance of long-range electrostatic interactions by surface charge retention protein-ATRP should be a general approach to enhancing the activity and stability of protein-polymer conjugates.

Supporting Information

Current PEGylation chemistries, charged ATRP initiator synthesis/characterization, MALDI-ToF data of proteins and protein-initiators, trypsin digestion data, IEF gel, DLS distributions, residual activity of CT-mixed initiator, MD simulation data (radius of gyration, RMSD, total energy), salt bridge analysis, and deactivation rates from residual activities.

AUTHOR CONTRIBUTIONS

H.M. synthesized and characterized the ATRP-initiators, protein-initiators and protein-polymer conjugates. H.M. also performed activity and stability measurements for the increased scope of proteins. S.L.B. performed the CT, CT-initiators, and CT-polymer conjugate Michaelis-Menten activities and stabilities. S.L.B. also performed trypsin digestions, MALDI-ToF acquisition, running of the IEF gel, and the molecular dynamics simulation. B.K. and A.T. synthesized avidin conjugates and performed avidin activity assays. S.L.B. drafted the manuscript and A.J.R. and K.M. supervised the project and provided guidance.

ACKNOWLEDGEMENTS

We would like to thank Adam Wood for discussion about the electric field strength, Weihang Ji for assistance with IEF gels, and Libin Zhang for assistance with ESI-MS.

FUNDING

The authors acknowledge financial support provided by Carnegie Mellon University Center for Polymer-Based Protein Engineering and DTRA grant: HDTRA1-18-1-0028 Carnegie Mellon FRBAA14-BR-TA7-G19-2-0124.

NOTES

The authors declare no competing financial interests.

Correspondence and request for materials should be addressed to alanrussell@cmu.edu.

REFERENCES

(1) Taverna, D. M.; Goldstein, R. A. Why Are Proteins Marginally Stable? *Proteins* **2002**, *46* (1), 105–109.

(2) Calligari, P. A.; Calandrini, V.; Ollivier, J.; Artero, J.-B.; Härtlein, M.; Johnson, M.; Kneller, G. R. Adaptation of Extremophilic Proteins with Temperature and Pressure: Evidence from Initiation Factor 6. *J. Phys. Chem. B* **2015**, *119* (25), 7860–7873.

(3) de Champdoré, M.; Staiano, M.; Rossi, M.; D'Auria, S. Proteins from Extremophiles as Stable Tools for Advanced Biotechnological Applications of High Social Interest. *J. R. Soc. Interface* **2007**, *4* (13), 183–191.

(4) Coker, J. A. Extremophiles and Biotechnology: Current Uses and Prospects. *F1000Research* **2016**, *5*.

(5) Radestock, S.; Gohlke, H. Exploiting the Link between Protein Rigidity and Thermostability for Data-Driven Protein Engineering. *Eng. Life Sci.* **2008**, *8* (5), 507–522.

(6) Abuchowski, A.; Mccoy, J. R.; Palczuk, N. C.; van Es, T.; Davis, F. F. Effect of Covalent Attachment of Polyethylene Glycol on Immunogenicity and Circulating Life of Bovine Liver Catalase *. *J. Biol. Chem.* **1976**, *252* (11), 3582–3586.

(7) Abuchowski, A.; van Es, T.; Palczuk, N. C.; Davis, F. F. Alteration of Immunological Properties of Bovine Serum Albumin by Covalent Attachment of Poly(ethylene Glycol). *J. Control. Rel.* **1977**, *252* (11), 3578–3581.

(8) Lele, B. S.; Murata, H.; Matyjaszewski, K.; Russell, A. J. Synthesis of Uniform Protein-

Polymer Conjugates. *Biomacromolecules* **2005**, *6* (6), 3380–3387.

(9) Cummings, C. S.; Campbell, A. S.; Baker, S. L.; Carmali, S.; Murata, H.; Russell, A. J. Design of Stomach Acid-Stable and Mucin-Binding Enzyme Polymer Conjugates. *Biomacromolecules* **2017**, *18* (2), 576–586.

(10) Murata, H.; Cummings, C. S.; Koepsel, R. R.; Russell, A. J. Polymer-Based Protein Engineering Can Rationally Tune Enzyme Activity, pH-Dependence, and Stability. *Biomacromolecules* **2013**, *14* (6), 1919–1926.

(11) Veronese, F. M.; Pasut, G. PEGylation, Successful Approach to Drug Delivery. *Drug Discov. Today* **2005**, *10* (21), 1451–1458.

(12) Parrott, M. C.; DeSimone, J. M. Drug Delivery: Relieving PEGylation. *Nat. Chem.* **2011**, *4* (1), 13–14.

(13) Huang, A.; Qin, G.; Olsen, B. D. Highly Active Biocatalytic Coatings from Protein-Polymer Diblock Copolymers. *ACS Appl. Mater. Interfaces* **2015**, *7* (27), 14660–14669.

(14) Campbell, A. S.; Islam, M. F.; Russell, A. J. Intramolecular Electron Transfer through Poly-Ferrocenyl Glucose Oxidase Conjugates to Carbon Electrodes: 1. Sensor Sensitivity, Selectivity and Longevity. *Electrochim. Acta* **2017**, *248*, 578–584.

(15) Shakya, A. K.; Nandakumar, K. S. An Update on Smart Biocatalysts for Industrial and Biomedical Applications. *J. R. Soc. Interface* **2018**, *15*, 1–15.

(16) Cummings, C. S.; Campbell, A. S.; Baker, S. L.; Carmali, S.; Murata, H.; Russell, A. J. Design of Stomach Acid-Stable and Mucin-Binding Enzyme Polymer Conjugates. *Biomacromolecules* **2017**, *18* (2), 576–586.

(17) Lozano, P.; de Diego, T.; Guegan, J. P.; Vaultier, M.; Iborra, J. L. Stabilization of Alpha-Chymotrypsin by Ionic Liquids in Transesterification Reactions. *Biotechnol. Bioeng.* **2001**,

75 (5), 563–569.

(18) Heredia, K. L.; Bontempo, D.; Ly, T.; Byers, J. T.; Halstenberg, S.; Maynard, H. D. In Situ Preparation of Protein - "Smart" polymer Conjugates with Retention of Bioactivity. *J. Am. Chem. Soc.* **2005**, *127* (48), 16955–16960.

(19) Heredia, K. L.; Maynard, H. D. Synthesis of Protein-Polymer Conjugates. *Org. Biomol. Chem.* **2007**, *5* (1), 45–53.

(20) Bontempo, D.; Maynard, H. D. Streptavidin as a Macroinitiator for Polymerization: In Situ Protein−Polymer Conjugate Formation. *J Am Chem Soc* **2005**, *127* (18), 6508–6509.

(21) Matyjaszewski, K.; Tsarevsky, N. V. Macromolecular Engineering by Atom Transfer Radical Polymerization. *J. Am. Chem. Soc.* **2014**, *136* (18), 6513–6533.

(22) Averick, S.; Simakova, A.; Park, S.; Konkolewicz, D.; Magenau, A. J. D.; Mehl, R. A.; Matyjaszewski, K. ATRP under Biologically Relevant Conditions: Grafting from a Protein. *ACS Macro Lett.* **2012**, *1* (1), 6–10.

(23) Panganiban, B.; Qiao, B.; Jiang, T.; DelRe, C.; Obadia, M. M.; Nguyen, T. D.; Smith, A. A. A.; Hall, A.; Sit, I.; Crosby, M. G.; et al. Random Heteropolymers Preserve Protein Function in Foreign Environments. *Science* **2018**, *359* (6381), 1239–1243.

(24) Kulkarni, S.; Schilli, C.; Grin, B.; Müller, A. H. E.; Hoffman, A. S.; Stayton, P. S. Controlling the Aggregation of Conjugates of Streptavidin with Smart Block Copolymers Prepared via the RAFT Copolymerization Technique. *Biomacromolecules* **2006**, *7* (10), 2736–2741.

(25) Huang, A.; Qin, G.; Olsen, B. D. Highly Active Biocatalytic Coatings from Protein–Polymer Diblock Copolymers. *ACS Appl. Mater. Interfaces* **2015**, *7* (27), 14660–14669.

(26) Cummings, C.; Murata, H.; Koepsel, R.; Russell, A. J. Dramatically Increased pH and

Temperature Stability of Chymotrypsin Using Dual Block Polymer-Based Protein Engineering. *Biomacromolecules* **2014**, *15* (3), 763–771.

(27) Trzebicka, B.; Szweda, R.; Kosowski, D.; Szweda, D.; Otulakowski, Ł.; Haladjova, E.; Dworak, A. Thermoresponsive Polymer-Peptide/protein Conjugates. *Prog. Polym. Sci.* **2017**, *68*, 35–76.

(28) Cummings, C.; Murata, H.; Koepsel, R.; Russell, A. J. Tailoring Enzyme Activity and Stability Using Polymer-Based Protein Engineering. *Biomaterials* **2013**, *34* (30), 7437–7443.

(29) Gauthier, M. a.; Klok, H.-A. Polymer–protein Conjugates: An Enzymatic Activity Perspective. *Polym. Chem.* **2010**, *1* (9), 1352.

(30) Lucius, M.; Falatach, R.; McGlone, C.; Makaroff, K.; Danielson, A.; Williams, C.; Nix, J. C.; Konkolewicz, D.; Page, R. C.; Berberich, J. A. Investigating the Impact of Polymer Functional Groups on the Stability and Activity of Lysozyme-Polymer Conjugates. *Biomacromolecules* **2016**, *17* (3), 1123–1134.

(31) Bhattacharjee, S.; Liu, W.; Wang, W. H.; Weitzhandler, I.; Li, X.; Qi, Y.; Liu, J.; Pang, Y.; Hunt, D. F.; Chilkoti, A. Site-Specific Zwitterionic Polymer Conjugates of a Protein Have Long Plasma Circulation. *ChemBioChem* **2015**, *16* (17), 2451–2455.

(32) Baker, S. L.; Munasinghe, A.; Murata, H.; Lin, P.; Matyjaszewski, K.; Colina, C. M.; Russell, A. J. Intramolecular Interactions of Conjugated Polymers Mimic Molecular Chaperones to Stabilize Protein–Polymer Conjugates. *Biomacromolecules* **2018**, *19*, 3798–3813.

(33) Jevševar, S.; Kunstelj, M.; Porekar, V. G. PEGylation of Therapeutic Proteins. *Biotechnol. J.* **2010**, *5* (1), 113–128.

(34) Russell, A. J.; Baker, S. L.; Colina, C. M.; Figg, C. A.; Kaar, J. L.; Matyjaszewski, K.; Simakova, A.; Sumerlin, B. S. Next Generation Protein-Polymer Conjugates. *AIChE J.* **2018**, *00* (0), 1–16.

(35) Keefe, A. J.; Jiang, S. Poly(zwitterionic)protein Conjugates Offer Increased Stability without Sacrificing Binding Affinity or Bioactivity. *Nat. Chem.* **2011**, *4* (1), 59–63.

(36) Baldwin, R. L. How Hofmeister Ion Interactions Affect Protein Stability. *Biophys. J.* **1996**, *71* (4), 2056–2063.

(37) Pace, C. N.; Scholtz, J. M.; Grimsley, G. R. Forces Stabilizing Proteins. *FEBS Lett.* **2014**, *588* (14), 2177–2184.

(38) Dill, K. A. Dominant Forces in Protein Folding. *Biochemistry* **1990**, *29* (31), 7133–7155.

(39) Zhang, Z.; Witham, S.; Alexov, E. On the Role of Electrostatics in Protein-Protein Interactions. *Phys. Biol.* **2011**, *8* (3), 035001.

(40) Pace, C. N.; Shirley, B. A.; McNutt, M.; Gajiwala, K. Forces Contributing to the Conformational Stability of Proteins. *FASEB J.* **1996**, *10* (1), 75–83.

(41) Sanchez-Ruiz, J. M.; Makhatadze, G. I. To Charge or Not to Charge? *Trends Biotechnol.* **2001**, *19* (4), 132–135.

(42) Strickler, S. S.; Gribenko, A. V.; Gribenko, A. V.; Keiffer, T. R.; Tomlinson, J.; Reihle, T.; Loladze, V. V.; Makhatadze, G. I. Protein Stability and Surface Electrostatics: A Charged Relationship. *Biochemistry* **2006**, *45* (9), 2761–2766.

(43) Loladze, V. V; Ibarra-Molero, B.; Sanchez-Ruiz, J. M.; Makhatadze, G. I. Engineering a Thermostable Protein via Optimization of Charge-Charge Interactions on the Protein Surface. *Biochemistry* **1999**, *38*, 16419–16423.

(44) Marshall, S. A.; Morgan, C. S.; Mayo, S. L. Electrostatics Significantly Affect the

Stability of Designed Homeodomain Variants. *J. Mol. Biol.* **2002**, *316* (1), 189–199.

(45) Park, S.; Yang, X.; Saven, J. G. Advances in Computational Protein Design. *Curr. Opin. Struct. Biol.* **2004**, *14* (4), 487–494.

(46) Dwyer, M. A.; Looger, L. L.; Hellinga, H. W.; Misura, K.; Baker, D. Computational Design of a Biologically Active Enzyme. *Science (80-.).* **2004**, *304* (5679), 1967–1971.

(47) Chi-Fung Lee, George I. Makhatadze, and K.-B. W. Effects of Charge-to-Alanine Substitutions on the Stability of Ribosomal Protein L30e from Thermococcus Celer. *Biochemistry* **2005**, *44*, 16817–16825.

(48) Koide, A.; Jordan, M. R.; Horner, S. R.; Batori, V.; Koide, S. Stabilization of a Fibronectin Type III Domain by the Removal of Unfavorable Electrostatic Interactions on the Protein Surface. *Biochemistry* **2001**, *40* (34), 10326–10333.

(49) Loladze, V. V; Makhatadze, G. I. Removal of Surface Charge-Charge Interactions from Ubiquitin Leaves the Protein Folded and Very Stable. *Protein Sci.* **2002**, *11* (1), 174–177.

(50) Carmali, S.; Murata, H.; Amemiya, E.; Matyjaszewski, K.; Russell, A. J. Tertiary Structure-Based Prediction of How ATRP Initiators React with Proteins. *ACS Biomater. Sci. Eng.* **2017**, *3* (9), 2086–2097.

(51) Murata, H.; Carmali, S.; Baker, S. L.; Matyjaszewski, K.; Russell, A. J. Solid-Phase Synthesis of Protein-Polymers on Reversible Immobilization Supports. *Nat. Commun.* **2018**, *9*.

(52) Le Droumaguet, B.; Nicolas, J. Recent Advances in the Design of Bioconjugates from Controlled/living Radical Polymerization. *Polym. Chem.* **2010**, *1* (5), 563.

(53) Broyer, R. M.; Grover, G. N.; Maynard, H. D. Emerging Synthetic Approaches for Protein–polymer Conjugations. *Chem. Commun.* **2011**, *47* (8), 2212.

(54) Ui, N. Isoelectric Points and Conformation of Proteins II. Isoelectric Focusing of Alpha-Chymotrypsin and Its Inactive Derivative. *Biochim. Biophys. Acta* **1971**, *229*, 582–589.

(55) Isom, D. G.; Castañeda, C. A.; Cannon, B. R.; García-Moreno, B. Large Shifts in pKa Values of Lysine Residues Buried inside a Protein. *Proc. Natl. Acad. Sci. U. S. A.* **2011**, *108* (13), 5260–5265.

(56) Laurents, D. V.; Huyghues-Despointes, B. M. P.; Bruix, M.; Thurlkill, R. L.; Schell, D.; Newsom, S.; Grimsley, G. R.; Shaw, K. L.; Treviño, S.; Rico, M.; et al. Charge–Charge Interactions Are Key Determinants of the pK Values of Ionizable Groups in Ribonuclease Sa (pI=3.5) and a Basic Variant (pI=10.2). *J. Mol. Biol.* **2003**, *325* (5), 1077–1092.

(57) Murata, H.; Cummings, C. S.; Koepsel, R. R.; Russell, A. J. Rational Tailoring of Substrate and Inhibitor Affinity via ATRP Polymer-Based Protein Engineering. *Biomacromolecules* **2014**, *15* (7), 2817–2823.

(58) Rodríguez-Martínez, J. A.; Solá, R. J.; Castillo, B.; Cintrón-Colón, H. R.; Rivera-Rivera, I.; Barletta, G.; Griebenow, K. Stabilization of α-Chymotrypsin upon PEGylation Correlates with Reduced Structural Dynamics. *Biotechnol. Bioeng.* **2008**, *101* (6), 1142–1149.

(59) Lozano, P.; Combes, D.; Iborra, J. L. Effect of Polyols on Alpha-Chymotrypsin Thermostability: A Mechanistic Analysis of the Enzyme Stabilization. *J. Biotechnol.* **1994**, *35* (1), 9–18.

(60) Levitsky VYu; Panova, A. A.; Mozhaev, V. V. Correlation of High-Temperature Stability of Alpha-Chymotrypsin with “Salting-In” Properties of Solution. *Eur. J. Biochem.* **1994**, *219* (1-2), 231–236.

(61) Mozhaev, V. V.; Sergeeva, M. V.; Belova, A. B.; Khmelnitsky, Y. L. Multipoint

Attachment to a Support Protects Enzyme from Inactivation by Organic Solvents: α-Chymotrypsin in Aqueous Solutions of Alcohols and Diols. *Biotechnol. Bioeng.* **1990**, *35* (7), 653–659.

(62) Dorovska-Taran, V. N.; Veeger, C.; Visser, A. J. W. G. Comparison of the Dynamic Structure of Alpha-Chymotrypsin in Aqueous Solution and in Reversed Micelles by Fluorescent Active-Site Probing. *Eur. J. Biochem.* **1993**, *211* (1-2), 47–55.

(63) Lozano, P.; De Diego, T.; Iborra, J. L. Dynamic Structure/function Relationships in the Alpha-Chymotrypsin Deactivation Process by Heat and pH. *Eur. J. Biochem.* **1997**, *248* (1), 80–85.

(64) Williams, C.; Dougherty, M. L.; Makaroff, K.; Stapleton, J.; Konkolewicz, D.; Berberich, J. A.; Page, R. C. *Strategies for Biophysical Characterization of Protein–Polymer Conjugates*, 1st ed.; 2017; Vol. 590.

(65) Fersht, A. R. Conformational Equilibria in α- and δ-Chymotrypsin: The Energetics and Importance of the Salt Bridge. *J. Mol. Biol.* **1972**, *64* (2), 497–509.

(66) Cao, Z.; Jiang, S. Super-Hydrophilic Zwitterionic Poly(carboxybetaine) and Amphiphilic Non-Ionic Poly(ethylene Glycol) for Stealth Nanoparticles. *Nano Today* **2012**, *7* (5), 404–413.

(67) Shao, Q.; Jiang, S. Molecular Understanding and Design of Zwitterionic Materials. *Adv. Mater.* **2015**, *27* (1), 15–26.

(68) Liu, S.; Jiang, S. Zwitterionic Polymer-Protein Conjugates Reduce Polymer-Specific Antibody Response. *Nano Today* **2016**, *11* (3), 285–291.

(69) Kaupbayeva, B.; Murata, H.; Lucas, A.; Matyjaszewski, K.; Minden, J. S.; Russell, A. J. Molecular Sieving on the Surface of a Nano-Armored Protein. *Biomacromolecules* **2019**,

20 (3), 1235–1245.

(70) Girard, E.; Marchal, S.; Perez, J.; Finet, S.; Kahn, R.; Fourme, R.; Marassio, G.; Dhaussy, A.-C.; Prangé, T.; Giffard, M.; et al. Structure-Function Perturbation and Dissociation of Tetrameric Urate Oxidase by High Hydrostatic Pressure. *Biophys. J.* **2010**, *98* (10), 2365–2373.

(71) Gabison, L.; Prangé, T.; Colloc'h, N.; El Hajji, M.; Castro, B.; Chiadmi, M. Structural Analysis of Urate Oxidase in Complex with Its Natural Substrate Inhibited by Cyanide: Mechanistic Implications. *BMC Struct. Biol.* **2008**, *8* (1), 32.

(72) Colloc'h, N.; Prangé, T. Functional Relevance of the Internal Hydrophobic Cavity of Urate Oxidase. *FEBS Lett.* **2014**, *588* (9), 1715–1719.

(73) Axelsen, P. H.; Harel, M.; Silman, I.; Sussman, J. L. Structure and Dynamics of the Active Site Gorge of Acetylcholinesterase: Synergistic Use of Molecular Dynamics Simulation and X-Ray Crystallography. *Protein Sci.* **1994**, *3* (2), 188–197.

(74) Dvir, H.; Silman, I.; Harel, M.; Rosenberry, T. L.; Sussman, J. L. Acetylcholinesterase: From 3D Structure to Function. *Chem. Biol. Interact.* **2010**, *187* (1-3), 10–22.

Table of Contents Graphic

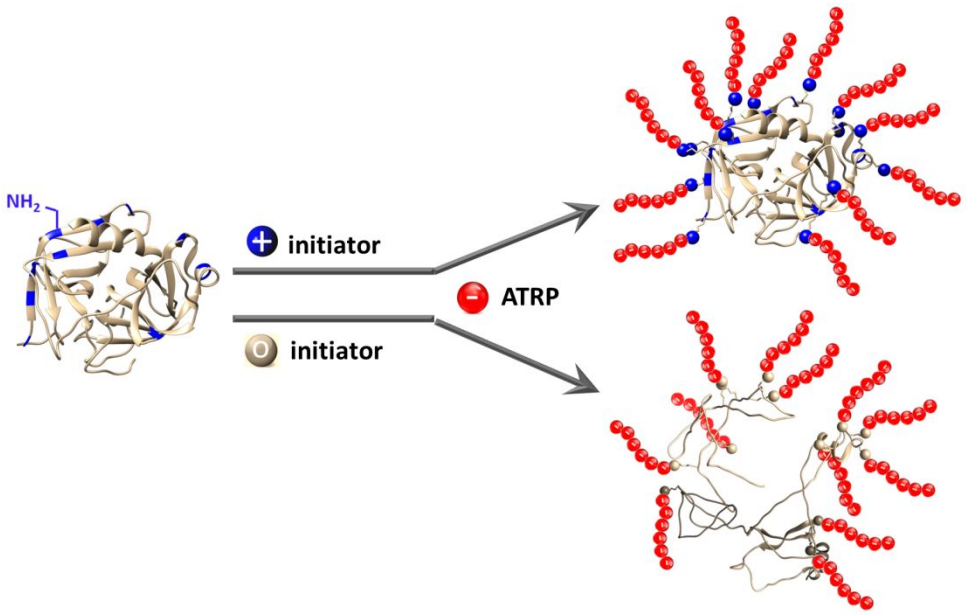

1106

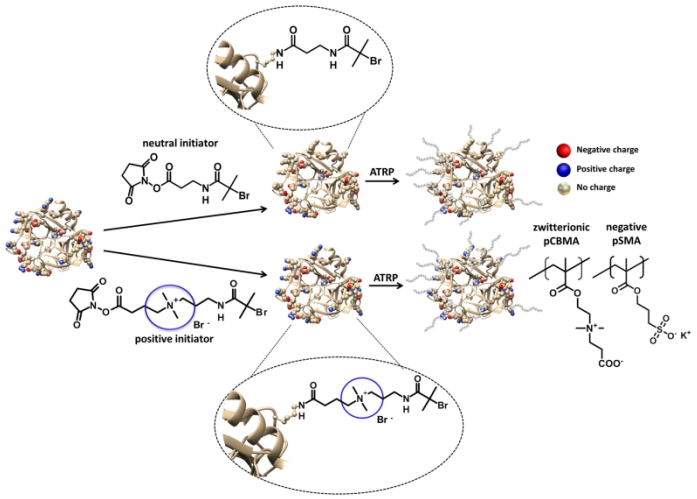

Scheme 1

380x190mm (205 x 205 DPI)

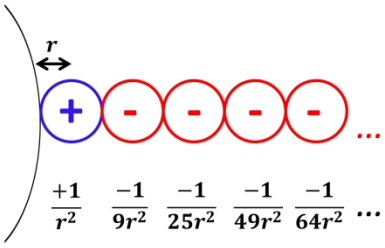

Figure 1

380x190mm (205 x 205 DPI)

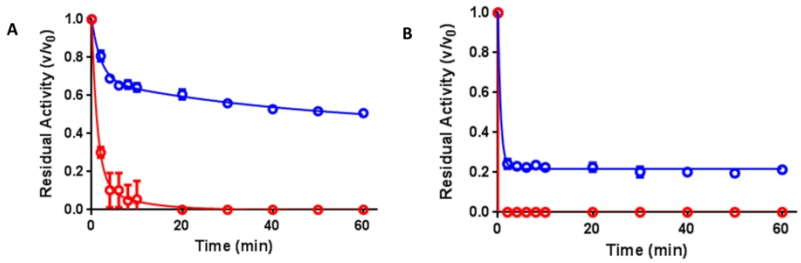

Figure 2

380x190mm (205 x 205 DPI)

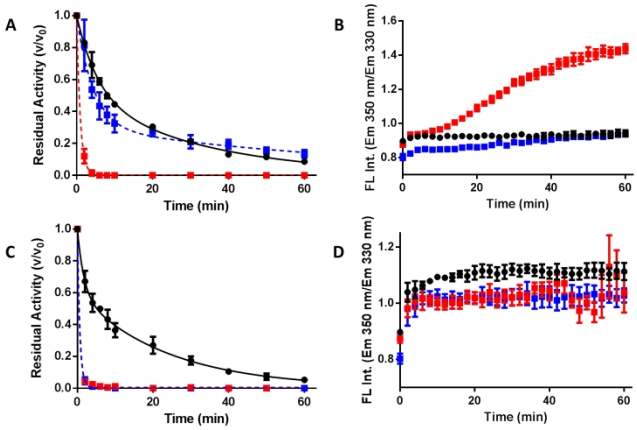

Figure 3

380x190mm (205 x 205 DPI)

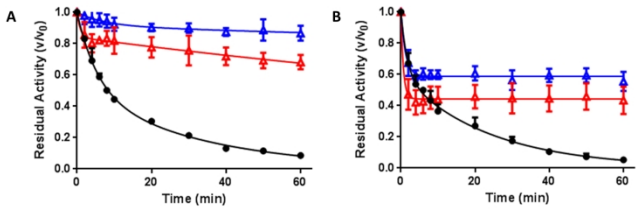

Figure 4

380x190mm (205 x 205 DPI)

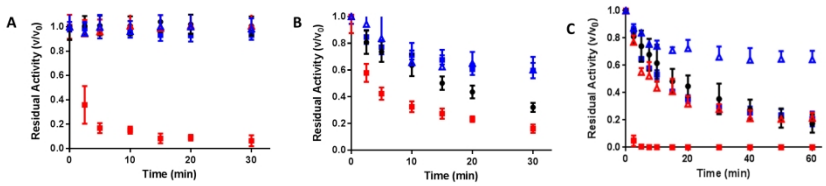

Figure 5

380x190mm (205 x 205 DPI)

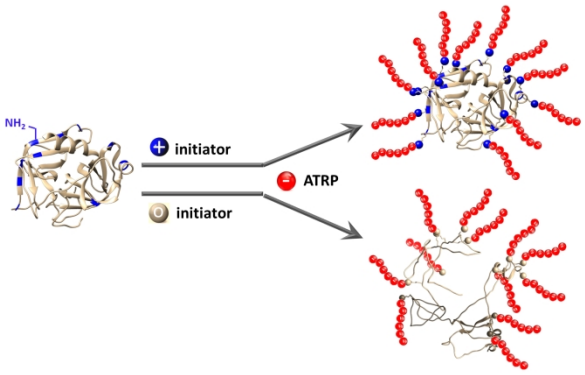

Table of Contents Figure

380x190mm (205 x 205 DPI)